EFFECTS OF SURFACE PLASMON EXCITATIONS ON PHOTOLUMINESCENCE BY CdSe/ZnS QUANTUM DOTS

by

ANKIT KUMAR SINGH

Presented to the Faculty of the Graduate School of

The University of Texas at Arlington in Partial Fulfillment

of the Requirements

for the Degree of

MASTER OF SCIENCE IN MATERIALS SCIENCE & ENGINEERING

THE UNIVERSITY OF TEXAS AT ARLINGTON

May 2013

ACKNOWLEDGEMENTS

I would like to express my gratitude to Professor Suresh C. Sharma for his guidance and support throughout this research work. His suggestions and questions made me think critically about the problems faced during the course of the research. This thesis would not have been possible without his persistent and invaluable guidance, as well as without the motivation provided by him. I enjoyed a lot working in his group as there was complete independence for implementation of novel ideas.

I would like to thank my fellow graduate student Mr. Kunal Tiwari for he was always there to support me. I would also like to thank Dr. Muhammed Yousufuddin, (Manager, Centre for Nanostructured Materials) for help with Raman measurements, Dr. Nader Hozhabri (Manager, Nanofab) for gold thin film deposition, and my colleague, Mr. Munuve Mwania for help with UV-VIS measurements.

I also thank Dr. Seong Jin Koh and Dr. Fuqiang Liu, Department of Materials Science & Engineering for serving on the Thesis Committee and for providing valuable suggestions.

Last but not the least, I am really thankful to my family members for their continuous support, encouragement and motivation without which, none of this would have been possible.

May 3, 2013

ABSTRACT

EFFECTS OF SURFACE PLASMON EXCITATIONS ON PHOTOLUMINESCENCE BY CdSe/ZnS QUANTUM DOTS

Ankit Kumar Singh, M.S

The University of Texas at Arlington, 2013

Supervising Professor: Suresh C. Sharma

The influence of localized surface plasmons (LSPs) and surface plasmon polaritons (SPPs) on the photoluminescence (PL) spectra of core/shell type CdSe/ZnS quantum dots (QDs) has been studied. Thin film samples of these QDs were deposited on glass slides, irradiated by 514 nm polarized beam from an Argon-ion laser, and PL spectra were measured using a high-resolution 1250M JY-Horiba spectrometer equipped with liquid-nitrogen cooled CCD detector. In the first set of experiments, PL spectra were measured on QDs and QDs-Au NPs mixture as a function of the intensity of the 514 nm laser beam. In the second set of experiments, PL spectra were measured by using Kretschmann geometry, in which the SPPs were excited by p-polarized 514 nm laser beam incident upon a high-index prism coated with a 35 nm Au film. The films of QDs were deposited over the Au film by dissolving them in chloroform. Modified arrangement for Kretschmann configuration has been used and its advantages over other conventional arrangements have been discussed.

TABLE OF CONTENTS

LIST OF ILLUSTRATIONS

Figure Page

LIST OF TABLES

CHAPTER 1

INTRODUCTION

Surface Plasmons (SPs) are coherent oscillation of electron cloud existing between the interfaces of two different materials where there is a change in the sign of real part of dielectric. For example, a metal-dielectric interface. When these SPs are coupled with photons, they are called surface plasmon polaritons (SPPs) which can propagate along the interface until all their energy gets lost into the surrounding environment. These SPPs can be easily created using visible radiation and a thin metal film in Kretschmann geometry [1]. In case when the interface is confined into a small volume, like those of metal nanoparticles, the SPs created cannot propagate along any particular direction. Thus, the plasmons created in metal nanostructures which are localized into a certain volume are called Localized Surface Plasmons (LSPs).

Metals like Gold (Au) and Silver (Ag) exhibit localized surface plasmon resonance (LSPR) in visible range of radiation which arises from the collective oscillation of electron clouds on the surface of their nanostructures [2-7]. Localized surface plasmons (LSPs) can be created by the interaction between nanoparticles of these metals. These LSPs have the potential to increase the Photoluminescence (PL) of a light emitting material kept in the proximity of these nanoparticles [8]. LSPs are also known to enhance the Raman signal by Surface Enhanced Raman Scattering (SERS) phenomenon [4-6]. LSPs have been intensively studied in the field of photonics and plasmonics [9-11].

Thus, the potential of LSPs can be exploited to enhance the luminescence from light emitting semiconductor quantum dots (QDs) such as CdSe/ZnS. CdSe/ZnS QDs are photoluminescent zero dimensional nanostructures with narrow spectral bandwidth and tunable band structure that can be easily controlled by monitoring their shape and size at the time of manufacturing [12-14]. These QDs are amongst the topmost candidates for nanoscale

optoelectronic devices such as lasers, light emitting diodes and solar cells [15-17]. The response of charge carriers in these QDs can be controlled using charge and energy transfer at the interface between their surface and the surrounding environment.

In this work, a series of experiments have been carried out to study the PL response of CdSe/ZnS QDs in presence of LSPs and SPPs.

CHAPTER 2

THEORY

2.1 Quantum Dots (QDs)

The history of QDs starts back in the 1970s and 1980s, when the solid state physicists began investigating quantum structures. The earliest structure of such kind was quantum well [18, 19]. These quantum wells consisted of a thin layer, about 10 nm, of semiconducting material sandwiched between insulating materials of much larger thickness. When this semiconducting layer absorbs a photon, an electron is promoted from valence band to conduction band, thus creating an electron-hole pair. Due to the sandwich structure, these charge carriers are constrained to move along the direction perpendicular to the surface of the sandwiched semiconductor. However, these carriers can move freely along the other two dimensions. Thus, this structure behaves as a quantum well with infinite potential walls along the insulating material. Quantum wells are also referred as two dimensional systems.

The properties of the nanostructures are greatly affected by their shape. As compared to the bulk, reducing any of the dimensions to confine the charge carriers results in change of the band structure [20]. Their electronic characteristics are closely related to the shape and size of the individual crystal. Larger the confinement potential of the crystal i.e. smaller the spatial dimensions, larger will be the shift in band gap energy. Thus, crystals with smaller size have larger band gap resulting into requirement of higher energy for excitation and subsequently, emission of higher energy while returning back to the ground state. This means that their electronic properties can be tuned by controlling their size. A QD is a zero dimensional system which has electron-hole pairs confined in all the three dimensions. Their

electronic properties are intermediate between those of bulk material and an individual atom/molecule [21]. Hence, they are often termed as artificial atoms.

2.1.1 Core/Shell Quantum Dots

The optical properties of these QDs are greatly dependent on their bulk and surface configurations. Because of their small size, their surface to volume ratio is very large. This means that the properties of their surface will play a crucial role in the overall properties of the QD crystal. In a single QD crystal, the surface atoms are not completely bonded to the inner bulk resulting into free dangling bonds at their surface. These dangling bonds act as trapping sites for electrons and holes created during excitation of the crystal which ultimately results in decreased quantum efficiency. This problem of charge carrier trapping can be minimized by coating of the surface with another material. One way is to use organic ligands to bind these dangling bonds and the other better way s to grow an epitaxial-like shell of inorganic material onto the core of the QDs [22]. This hybrid crystal, as shown in figure 2.1, is called as Core/Shell Quantum Dot. This shell also protects the core from outer electric field effects. The thickness and composition of the shell can be adjusted to get different band gaps. Thus, addition of shell allows the tunability of the emission spectra over a wider range of wavelengths than that available with the individual materials [22].

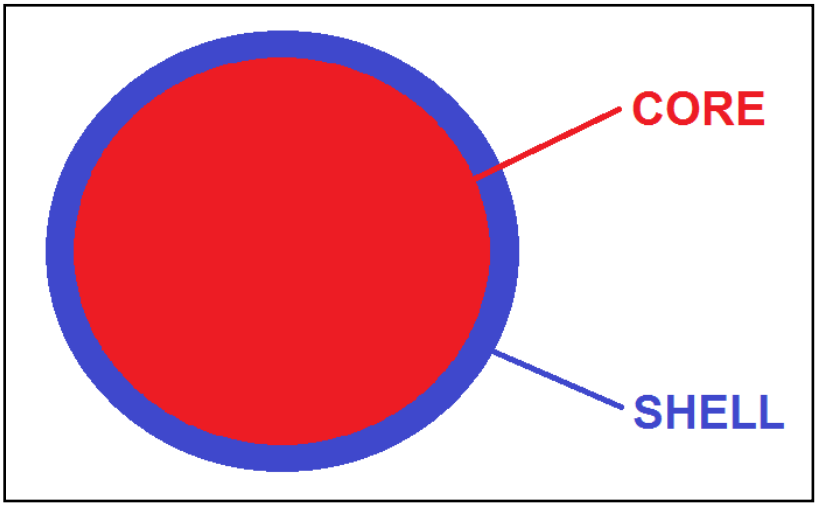

Figure 2.1 Schematic diagram representing Core/Shell Quantum Dots [23]

Based on their band alignment, these core/shell quantum dots can be classified into three categories as following [22]

2.1.1.1 Type I

In this category, the band gap of the shell is larger than that of the core such that the charge carriers, electrons and holes, both are confined in the core itself i.e. the edges of conduction and valence bands of the core lies within those of the shell, as shown in figure 2.2. For ex CdSe/CdS and CdSe/ZnS [24].

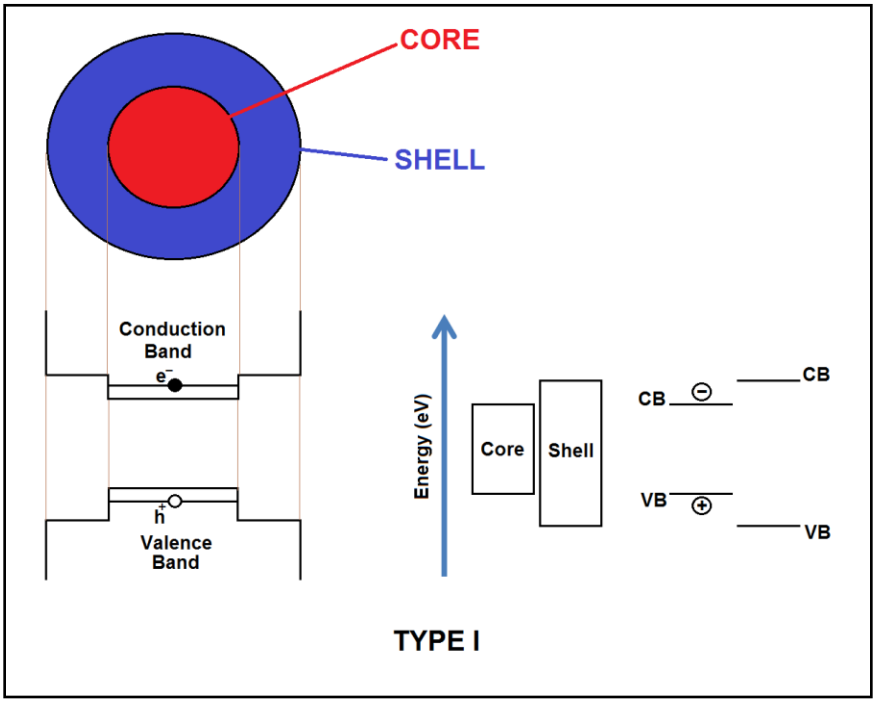

Figure 2.2 Type I Core/Shell Quantum Dots [24, 25]

2.1.1.2 Reverse Type I

In this category, unlike Type I, the core has larger band gap than the shell, and the edges of the conduction and valence bands of the shell lies within those of the core and, the charge carriers are either fully or partially confined into the shell material, as shown in figure 2.3. For ex CdS/CdSe and ZnSe/CdSe [24].

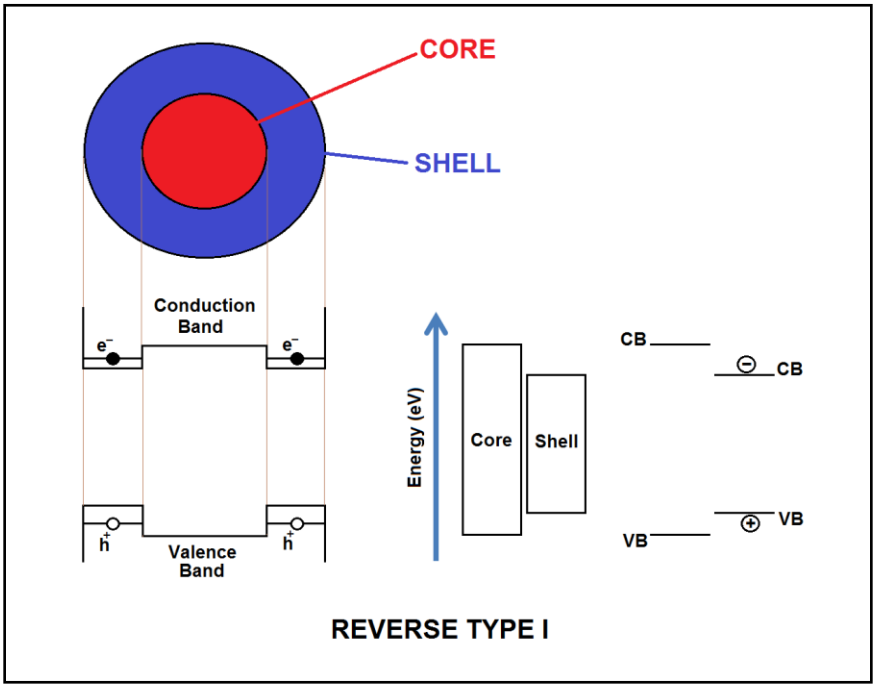

Figure 2.3 Reverse Type I Core/Shell Quantum Dots [24, 25]

2.1.1.3 Type II

In this category, the edges of the conduction band and valence band of the core are both either higher or lower than those of the conduction band and valence band of the shell, as shown in figure 2.4. In this case, the overall band gap is lower than the individual band gaps and the charge carriers are confined in this reduced band gap. For ex CdTe/CdSe and ZnTe/CdSe [24].

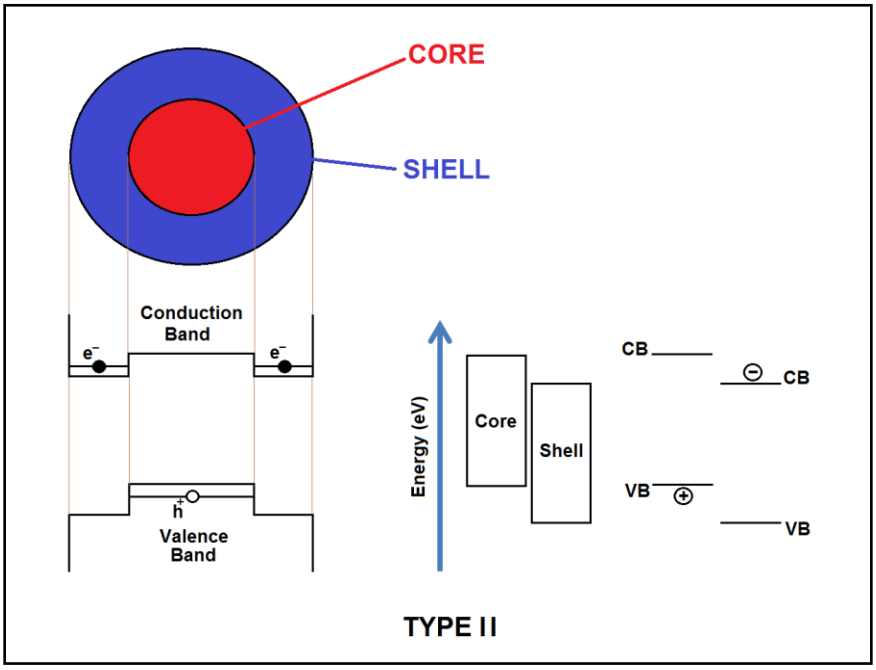

Figure 2.4 Type II Core/Shell Quantum Dots [24, 25]

2.2 Photoluminescence (PL)

PL is a process in which a material absorbs higher energy photons and emits either the same energy or lower energy photons. This can also be described as the excitation of the material to a higher energy state and then, relaxation to a lower energy state along with emission of a photon. The time gap between absorption and emission of photons is usually in the order of few nanoseconds which can be increased to hours depending upon applied conditions. While being in excited state, the material can undergo internal energy transition before the emission of lower energy radiation. Some of the energy from the incident photon is lost during this transition and thus, the emitted photon has lower energy and hence, larger wavelength as compared to the incident photon. This change in wavelength is called as red shift. This phenomenon can be described using Jablonski diagram, as shown in figure 2.5 [26].

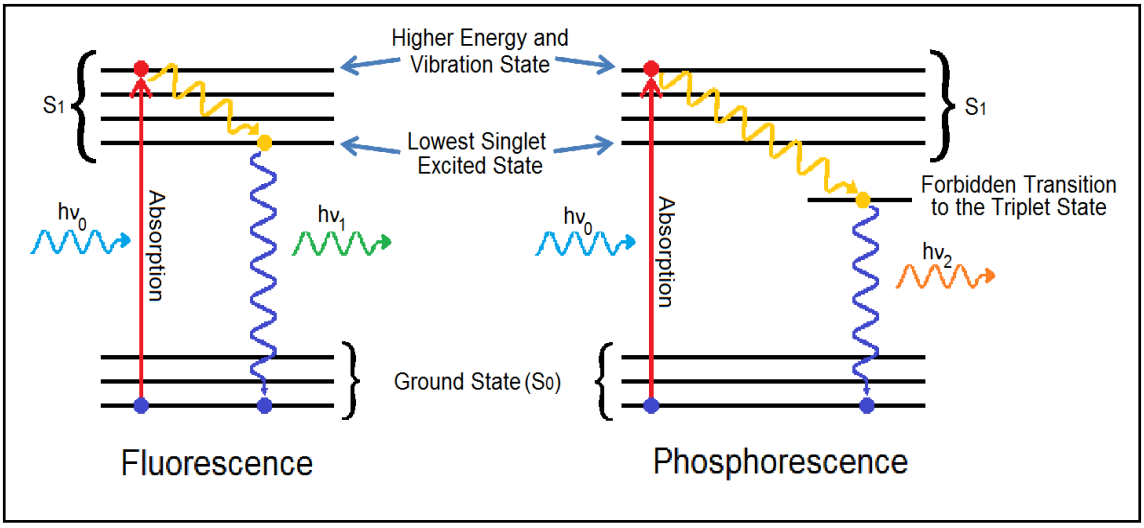

Figure 2.5 Jablonski Diagram [26]

In the above diagram, the set of lines represent a particular energy states and the parallel lines in a set represent different vibrational energy states. The colored circles represent electron undergoing transition. When this electron absorbs a photon with sufficient energy, it gets excited to the higher energy state (S_1) from ground state (S_0). It then undergoes internal conversion and rapidly relaxes to lowest singlet excited state. From this state, it comes back to the ground state emitting the extra energy in the form of a photon having energy less than the one which was absorbed. This process is called Fluorescence. However, in some cases, the excited electron in the higher energy state (S_1) undergoes intersystem crossing into a forbidden triplet state having higher spin multiplicity. As this state is quantum mechanically unfavorable, the electron transition from this state to the ground state is slower than that of the fluorescence. When the electron comes back to the ground state from this forbidden triplet state, it emits photon which usually has lesser energy as compared to that of the fluorescence. This process is called Phosphorescence [27].

2.3 Plasmons

Plasmons can be described as free electron density oscillations with respect to the fixed positive ions in metals. If an electric field is applied across a metal in a particular direction, the electrons get aligned in the opposite direction and when the field is reversed, the electrons align themselves in the opposite direction. This oscillation of electron cloud, as shown in figure 2.6, depends upon the application of electric field and Plasmons are quantization of these oscillations [28].

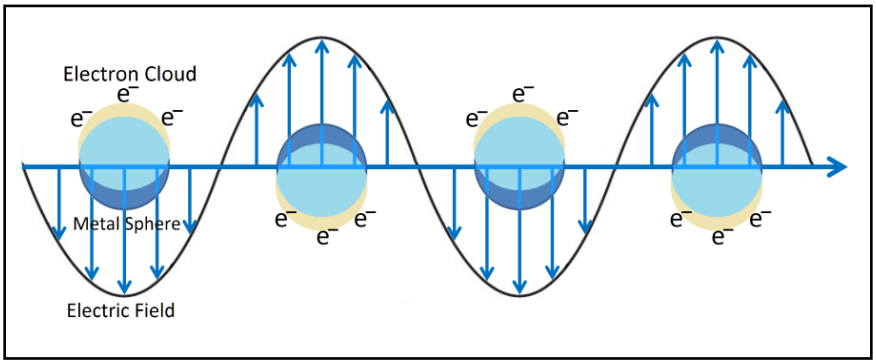

Figure 2.6 Oscillation of metal electron cloud in presence of photon associated electric field [29]

In case of metals, plasmons play a critical role in terms of their optical properties. Photons with frequency lesser than plasma frequency get reflected from the metal surface as the electrons in the metal act as screen for the electric field of photons. On the other hand, photons with higher frequency than plasma frequency get transmitted as the electrons cannot respond fast enough to the electric field of the photons so as to screen them. Most of the metals have plasma frequency in ultra violet range making them shiny and reflective in visible range. Some of the metals like gold and copper have electronic transitions in visible range due to which specific energy photons are absorbed thereby imparting color to these metals. For semiconductors, their valence electron plasma frequency is, in most cases, in ultraviolet range which makes them also reflective to visible radiations [28].

Plasmon energy can be estimated using the free electron model as following

$$E_p = \hbar\sqrt{\frac{ne^2}{m\epsilon_0}} = \hbar\omega_p$$

Where, n = conduction electron density, e = electron charge, m = mass of electron, ε_0 = free space permittivity, ħ = reduced Planck constant and ω_p = plasmon frequency

The existence of plasmons is a result of the interaction between metal nanostructures and photons. At optical frequencies, the free electrons in metal can sustain surface and volume charge density oscillations, called as surface plasmons and bulk plasmons, respectively.

2.3.1 Surface Plasmons

Coherent electron oscillations, existing at the interface between any two materials where there is change in the sign of real part of the dielectric function across the interface, are termed as Surface Plasmons. An example of such interface is a metal-dielectric interface where the real part of dielectric function changes sign from positive to negative when we go from dielectric to metal. Surface plasmons, as shown in figure 2.7, have lower energy than those of bulk plasmons, in which the longitudinal electron oscillations about the positive ion core within the bulk of an electron gas are quantized [28].

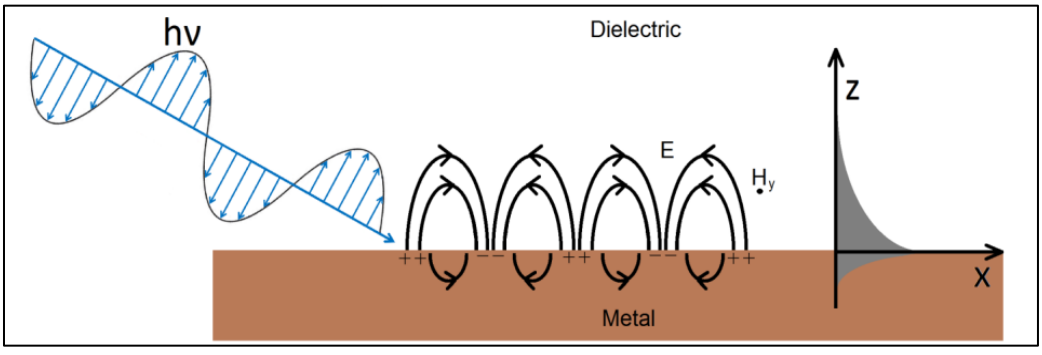

Figure 2.7 Surface Plasmon Polaritons [30]

2.3.2 Surface Plasmon Polaritons

The hybridized excitation resulting from the coupling of surface plasmons with photons are called Surface Plasmon Polaritons (SPPs). These SPPs are collective longitudinal oscillation of electrons near the metal surface coupled strongly with an electromagnetic wave. They can propagate for long distances along the surface of the metal until all the energy is lost, due to absorption in the metal or radiated into the surrounding environment. Their existence was first predicted by David Pines [31] and Rufus Ritchie [32].

The electromagnetic wave associated with surface plasmons has both transverse and longitudinal field components. These can only be excited at metal-dielectric interface and are bound tightly to the surface. The fields reach their maximum at the intersection of the surfaces and then decay exponentially away from the surfaces as shown in fig. 7.

2.3.3 Derivation of Bulk and Surface Plasmons

Bulk plasmons and Surface plasmons, both have associated electromagnetic waves that can be described by Maxwell's equations [28].

$$\vec{\nabla}.\vec{E} = \frac{1}{\varepsilon_0}\rho \tag{1}$$

$$\vec{\nabla}.\vec{B} = 0 \tag{2}$$

$$\vec{\nabla} \times \vec{E} = -\frac{\partial \vec{B}}{\partial t} = -\mu \frac{\partial \vec{H}}{\partial t} \tag{3}$$

$$\vec{\nabla} \times \vec{B} = \mu_0 \vec{J} + \mu_0 \varepsilon_0 \frac{\partial \vec{E}}{\partial t} \tag{4}$$

The simplest model describing the motion of an electron in a conductor is a free electron driven by the field of electromagnetic wave as shown below

$$E(t) = E(\omega) e^{-i\omega t} \tag{5}$$

$$m_e \frac{d^2x}{dt^2} = -eE \tag{6}$$

$$x(t) = \frac{e}{m}\frac{1}{\omega^2}E(\omega)e^{-i\omega t} \quad (7)$$

Let us assume free electrons (figure 2.8) being acted upon by an electric field as shown below

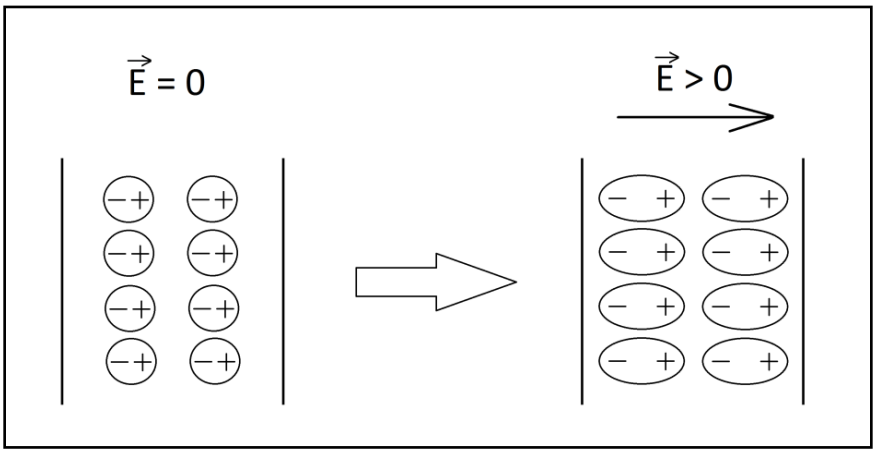

Figure 2.8 Polarization of charges inside metal

Due to the presence of applied electric field, the electrons get displaced and thus, the material gets polarized. Polarization of material is given by

$$\vec{p} = -ne\vec{\mu} \quad (8)$$

Where, $\vec{p}$ = polarization, n = number of electrons, e = electron charge, $\vec{\mu}$ = displacement of electrons

This displacement of free electrons follows Newton's law

$$\vec{F} = nm\frac{d^2\vec{\mu}}{dt^2} \quad (9)$$

$$-en\vec{E} = nm\frac{d^2\vec{\mu}}{dt^2} = \frac{nm}{ne}\frac{d^2\vec{p}}{dt^2}$$

$$\vec{E} = \frac{m}{ne^2}\frac{d^2\vec{p}}{dt^2} \tag{10}$$

Now for oscillating electric field ($\vec{E}$),

$$\vec{E} = \overrightarrow{E_0}(r)e^{-iwt}$$

$$\vec{p} = \overrightarrow{p_0}(r)e^{-iwt}$$

$$\frac{d^2\vec{p}}{dt^2} = -\omega^2\overrightarrow{p_0}(r)e^{-iwt} \tag{11}$$

Therefore,

$$\vec{E}(\vec{r},\omega) = -\frac{\omega^2 m}{ne^2}\vec{p}(\vec{r},\omega)$$

$$\vec{p}(\vec{r},\omega) = -\frac{ne^2}{\omega^2 m}\vec{E}(\vec{r},\omega)$$

Since,

$$\vec{D} = \epsilon_0\vec{E} + \vec{p} = \varepsilon_0\varepsilon\vec{E} \tag{12}$$

We get,

$$\vec{D}(\vec{r},\omega) = \varepsilon_0\vec{E}(\vec{r},\omega)\left[1 - \frac{ne^2}{\omega^2 m\varepsilon_0}\right] \tag{13}$$

From this equation, we obtain a frequency dependent dielectric permittivity

$$\varepsilon(\omega) = 1 - \frac{ne^2}{m\varepsilon_0}\left(\frac{1}{\omega^2}\right)$$

$$\omega_p^2 = \frac{ne^2}{m\varepsilon_0}$$

$$\varepsilon(\omega) = 1 - \left(\frac{\omega_p^2}{\omega^2}\right) \tag{14}$$

Where, m = electron mass, ω = frequency of applied electric field, ω_p = plasmon frequency, ε_0 = dielectric permittivity of free space, $\varepsilon(\omega)$ = free electron dielectric permittivity

Now,

$$v = f * \lambda$$

$$k = \frac{\omega}{v}$$

$$k = \frac{\omega}{c}\sqrt{\mu\varepsilon} \tag{15}$$

Equation (10) can be re-written as,

$$c^2k^2 = \omega^2 - \omega_p^2 \tag{16}$$

Equation (12) represents the dispersion relation for bulk plasmon polaritons propagating in the metallic film.

Figure 2.9 shows plot of the dispersion relation of bulk plasmons along with dispersion relation of free space ($\omega = ck$).

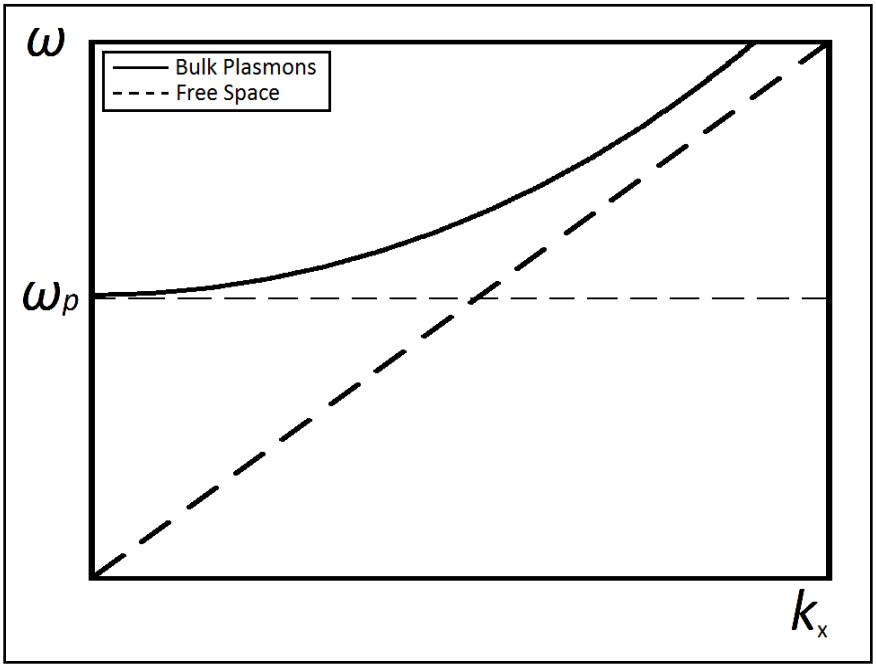

Figure 2.9 Dispersion relation for Bulk Plasmons [28]

Thus, the metal supports propagating waves for frequencies above plasma frequency. For frequencies below plasma frequency, k becomes imaginary and the evanescent fields thus generated, decay exponentially inside the metal. So, bulk plasmons which can exist deep inside the metal cannot exist for frequencies less than plasma frequency. Corresponding to these low frequencies, Surface plasmons are generated propagating along the interface between the metal and dielectric. The field intensity of this wave is at its maximum at the interface and decays exponentially away from the surface [28].

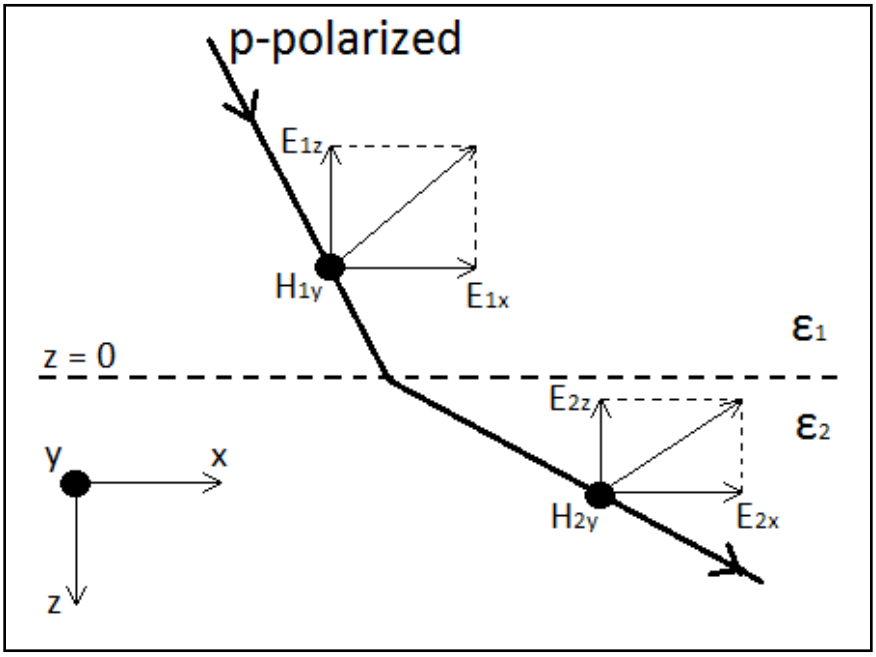

Figure 2.10 Propagation of p-polarized beam from denser medium to rarer medium [33]

Consider a p-polarized electromagnetic wave propagating from denser medium (ε_1) to rarer medium (ε_2) as shown in figure 2.10. The plane of interface is along x-y plane. The surface wave generated by this p-polarized electromagnetic wave has to satisfy the electromagnetic wave equation in both the media [33]. Thus, for the wave which is propagating only in the x-direction, we have

$$E_1 = (E_{x1}, 0, E_{z1})e^{i(k_x x - \omega t)}e^{ik_{z1}z} \quad (17)$$

$$H_1 = (0, H_{y1}, 0)e^{i(k_x x - \omega t)}e^{ik_{z1}z} \quad (18)$$

$$E_2 = (E_{x2}, 0, E_{z2})e^{i(k_x x - \omega t)}e^{ik_{z2}z} \quad (19)$$

$$H_2 = (0, H_{y2}, 0)e^{i(k_x x - \omega t)}e^{ik_{z2}z} \quad (20)$$

Applying Maxwell's equation (1), we get

$$\overrightarrow{E_{z1}} = -\overrightarrow{E_{x1}}\frac{k_x}{k_{z1}} \quad (21)$$

$$\overrightarrow{E_{z2}} = -\overrightarrow{E_{x2}}\frac{k_x}{k_{z2}} \tag{22}$$

The relationship between H_y and E_x can be determined using Maxwell's equation (3), which for $\mu = \mu_0$ gives

$$H_{y1} = \frac{\omega E_{x1}\varepsilon_1\varepsilon_0}{k_{z1}} \tag{23}$$

$$H_{y2} = \frac{\omega E_{x2}\varepsilon_2\varepsilon_0}{k_{z2}} \tag{24}$$

Applying boundary conditions at z=0, i.e. $H_{y1} = H_{y2}$ and $E_{y1} = E_{y2}$, we get

$$\frac{\varepsilon_1}{k_{z1}} = \frac{\varepsilon_2}{k_{z2}} \tag{25}$$

$$k_{z1} = -i(k_x^2 - \varepsilon_1 k^2)^{\frac{1}{2}} \tag{26}$$

$$k_{z2} = i(k_x^2 - \varepsilon_2 k^2)^{\frac{1}{2}} \tag{27}$$

For the wave to be truly a surface wave, that is trapped at the interface and decaying exponentially into both the media, we need $ik_{z1}>0$ and $ik_{z2}<0$. Thus, both k_{z1} and k_{z2} are imaginary and of opposite signs. Thus, ε_1 and ε_2 are of opposite sign as well. Substituting values from equation (26) & (27) in (25), we get

$$k_x = k\left(\frac{\varepsilon_1\varepsilon_2}{\varepsilon_1+\varepsilon_2}\right)^{\frac{1}{2}} = \frac{\omega}{c}\left(\frac{\varepsilon_1\varepsilon_2}{\varepsilon_1+\varepsilon_2}\right)^{\frac{1}{2}} \tag{28}$$

Considering, for dielectric, $\varepsilon_1 = 1$ and for metal, from equation (14), $\varepsilon_2 = 1 - \left(\frac{\omega_p^2}{\omega^2}\right)$, we get the following equation,

$$\omega^2 = \frac{\omega_p^2}{2} + (ck_x)^2 - \sqrt{(ck_x)^4 + \frac{\omega_p^4}{4}} \tag{29}$$

From equation (16) and (29), we get the following curve (figure 2.11) showing relation between ω and k.

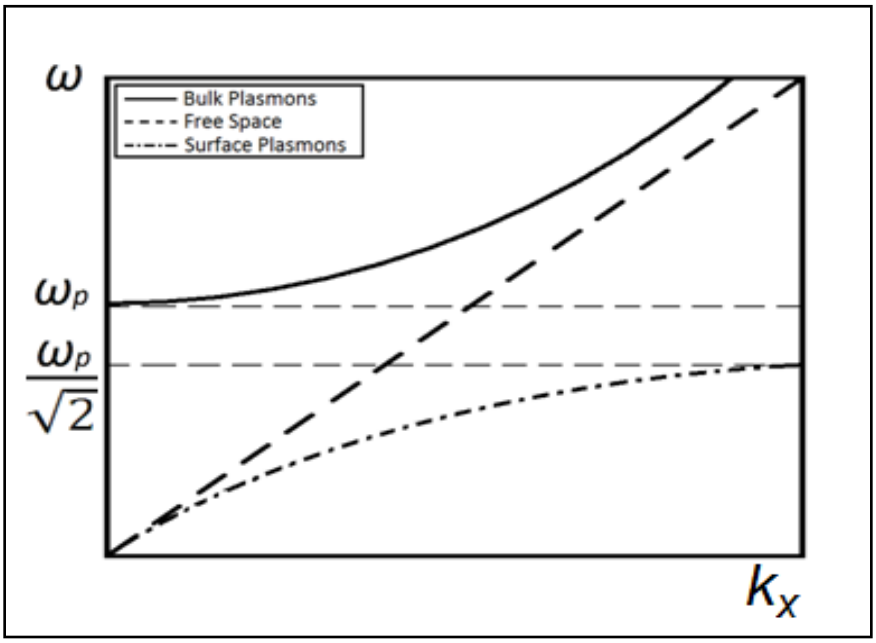

Figure 2.11 Dispersion relation for Surface Plasmons [28]

2.4 Excitation of Surface Plasmons

Excitation of surface plasmon waves using light is usually done through two well known configurations, namely, Kretschmann and Otto configurations [1, 34]. In Kretschmann configuration, a thin metal film is coated on the back of a prism or on glass and then, the glass is placed at the back of prism. When light illuminated the prism back or glass, after total internal reflection, the plasmons are excited at the outer side of the film as shown in figure 2.12.

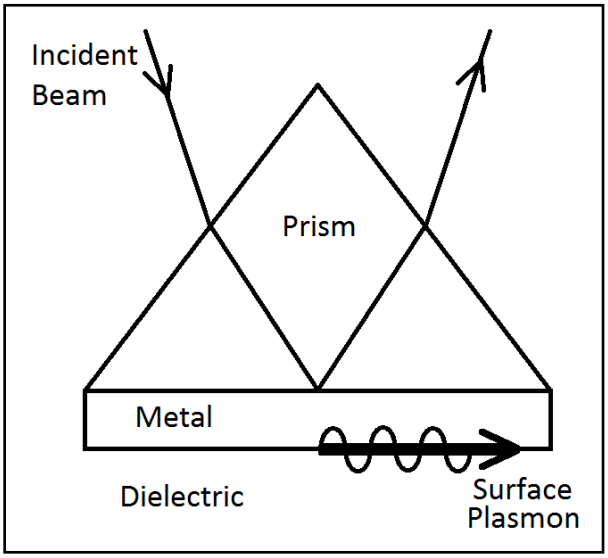

Figure 2.12 Kretschmann configuration [33]

In Otto configuration [34], the light illuminates the back side of the prism and gets totally internally reflected. A thin metal film is then brought in the proximity of the evanescent waves that are produced during total internal reflection and thus these evanescent waves interact with the plasma waves on metal film surface and excite the plasmons as shown in figure 2.13.

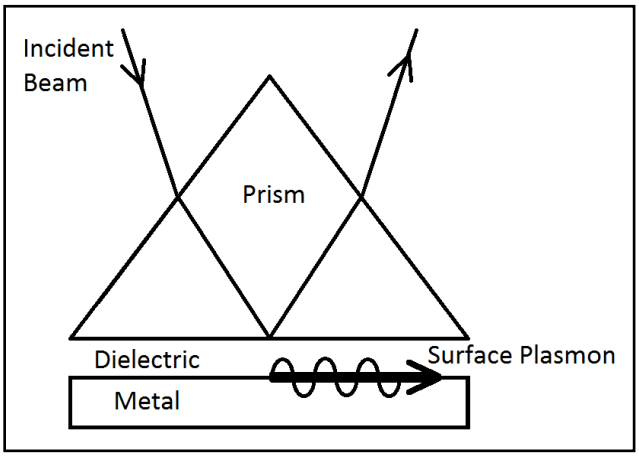

Figure 2.13 Otto configuration [33]

CHAPTER 3

EXPERIMENT

3.1 Preparation of samples

The CdSe/ZnS core/shell quantum dots (QDs) were purchased from Evident Technologies. Their average crystal diameter is ~5.2 nm, emission peak is centered at ~622 nm and have quantum yield of about 30-50% [35]. These QDs have added passivation of the outer ZnS shell by trioctylphosphine-oxide (TOPO) layer. The core of these QDs is comprised of CdSe having bandgap (E_g) of 1.7 eV and the shell is of ZnS having bandgap (E_g) of 3.68 eV at 300 K [36]. These core/shell structures come under the category (TYPE-I) of II-VI semiconductor nanocrystals (NCs). The holes are confined in the core (CdSe) due to passivation of the core surface by the shell (ZnS layer). However, the electron wavefunction extends into the shell. In case of additional layer of TOPO over the CdSe/ZnS, also called as capping TOPO layer, the dangling bonds at the outer surface of the ZnS layer get passivated which further enhances the photoluminescence and stability of these QDs. Thus, the final structure can be represented as CdSe/ZnS/TOPO. These QDs were used as is, without any further modification.

The first set of experiments was to determine the effect of gold (Au) nanoparticles (NPs) on the photoluminescence (PL) from these QDs. So, two samples were prepared. First sample was as received CdSe/ZnS QDs, named as Sample # 1. The second sample was prepared by mixing these QDs with Gold solution having Au NPs of size 14 nm and concentration of 10 ppm. This is named as Sample # 2.

The purpose of second set of experiments was to determine the effect of surface plasmons on PL from these QDs. So, for the creation of surface plasmons, a thin Au film of 35

nm was deposited at one of the faces of a high-index prism (refractive index (n_p) = 1.7847, 20mm equilateral Prism, N-SF11, uncoated, Edmund Optics). This particular face will be termed as base of the prism throughout this thesis. The Au film was deposited using sputtering. In order to observe PL of these QDs in presence of surface plasmons, a thin film of these QDs was to be deposited. So, these QDs were first dissolved in chloroform and then dropped over the base of the prism which is coated with Au film. Initially, the film formed was too thick for the creation of plasmons, which is discussed later. So, this thick film was then washed carefully several times, using chloroform and water, so that the thickness of this QD layer becomes so thin that surface plasmons can be created. The experiments were carried out using both of these QD films, thick and thin.

3.2 Experimental Setup for PL measurements

The optical system for PL measurements is shown in fig. 14. It consists of an Argon-ion Laser (Spectra Physics) emitting green laser beam at a wavelength of ~514 nm. This beam is first passed through a Band-pass filter which allows only 514 nm wavelength to pass through and all other wavelengths are attenuated. The beam is then passed through a narrow slit in order to get a collimated beam. Using mirrors, this collimated beam was made to be incident, at an inclined angle, over the sample placed on a glass slide. In order to study the effect of Au NPs on the PL, the intensity was varied using Optical Density (OD) filters (Edmund Optics, Absorptive ND Filter Kit #63-468). This OD filter was placed between two mirrors, as shown in figure 3.1. The surface of the OD filters was kept perfectly perpendicular to the beam direction because different OD filters have different thickness and while changing the filters, the position of beam spot, hitting the sample, might change in case the surface is at an inclined angle, other than normal.

After the beam hits the sample, the part of it gets transmitted, reflected and scattered through the sample and glass slide. Rest of it gets absorbed which produces PL at a wavelength of ~622 nm. Out of these, only scattered and PL wavelengths are considered

during the experiments. The laser beam gets scattered in all the directions. It is collected from the top of the sample using a microscope objective (Mitutoyo, 378-803-2, 10x, numerical aperture (NA) = 0.28, working distance (WD) = 33.5 mm). The height of this objective is adjusted such that the sample lies at its focal point. The PL coming out from the upper end of this objective is passed through a 50/50 beam splitter, which divides the collected beam into two parts, first of which goes into the video camera directly and the second part is headed towards the spectrometer. The video camera is connected to a computer which gets the live image of the sample, and was used to scan and fix the location of the objective at a particular position. The second part is then reflected from two mirrors aligned such that the beam hits the entrance slit of the spectrometer. Between the spectrometer and the mirror, an f/value matching lens is placed which focuses all the incident radiations at the aperture of the spectrometer to get the best possible result. The spectrometer used for the experiments is 1250M JY-Horiba Spectrometer which has liquid nitrogen cooled CCD for high sensitivity. The operating temperature of this CCD is 154 K. The grating used in this spectrometer is 1200 gratings/mm for high resolution. The spectrometer determines the wavelength distribution of the incoming radiation along with its intensity. This spectrometer is connected to a second computer which is used to operate it and collect the data. The PL from sample gets scattered in all directions and is collected and analyzed using the arrangement as above and the spectrometer is set with center position at 622 nm, which is in the proximity of the peak position of the PL. This is called as arrangement # 1 as shown in figure 3.1.

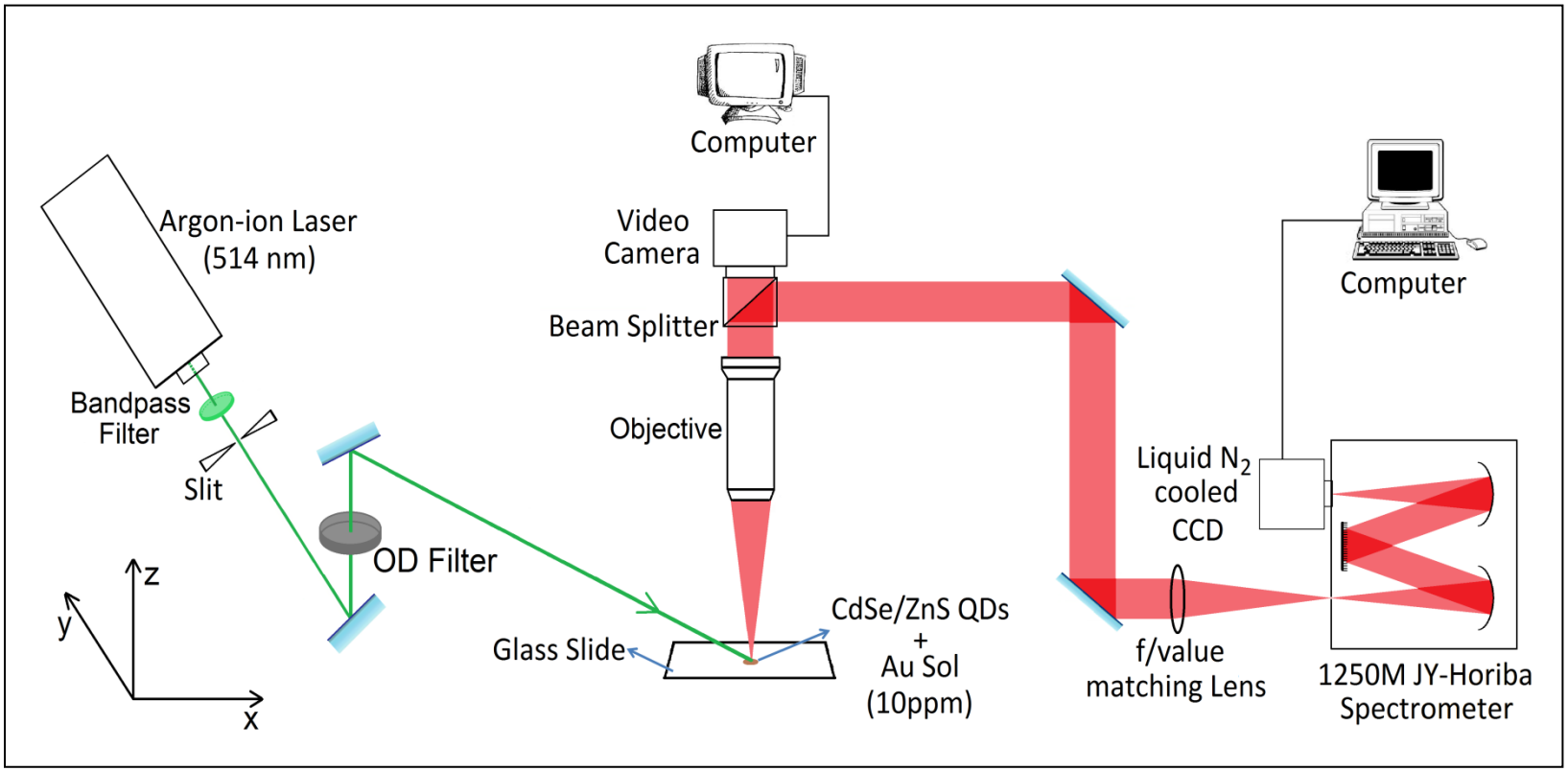

Figure 3.1 Experimental setup for PL intensity determination with variation in Incident intensity using OD filters

Since, combination (as shown in table 3.1) of available OD filters produced just a few data points (13 points); they were replaced by a polarizer (polarizer 1) as shown in figure 3.2. Figure 3.3 represents the variation in PL intensity with change in angle of polarizer 1. The laser itself is polarized in a particular direction. Hence, by changing the angle of polarizer 1, the intensity of laser beam changes. At the same time, the polarization of the beam hitting the sample also changes. This change in polarization angle might play an additional role in the PL behavior of the QDs. In order to avoid any effect from polarization change, another polarizer, termed as polarizer 2, was introduced before the sample and was kept at a fixed angle throughout the experiments. This ensures that whatever be the angle of polarization of polarizer 1, the beam hitting the sample will always remain polarized in the same direction as that of polarizer 2. Thus, the arrangements # 1 was modified using two polarizers into a new arrangement, termed as arrangement # 2, for the measurement of PL intensity (figure 3.2).

Table 3.1 Percentage Transmission from combination of OD filters

Filter	Optical Density (OD)	Transmission (%)
1	0.15	70.79458
2	0.2	63.09573
3	0.3	50.11872
4	0.4	39.81072
5	0.5	31.62278
6	0.6	25.11886
1+2	0.35	44.66836
1+3	0.45	35.48134
1+4	0.55	28.18383
1+5	0.65	22.38721
1+6	0.75	17.78279
2+3	0.5	31.62278
2+4	0.6	25.11886

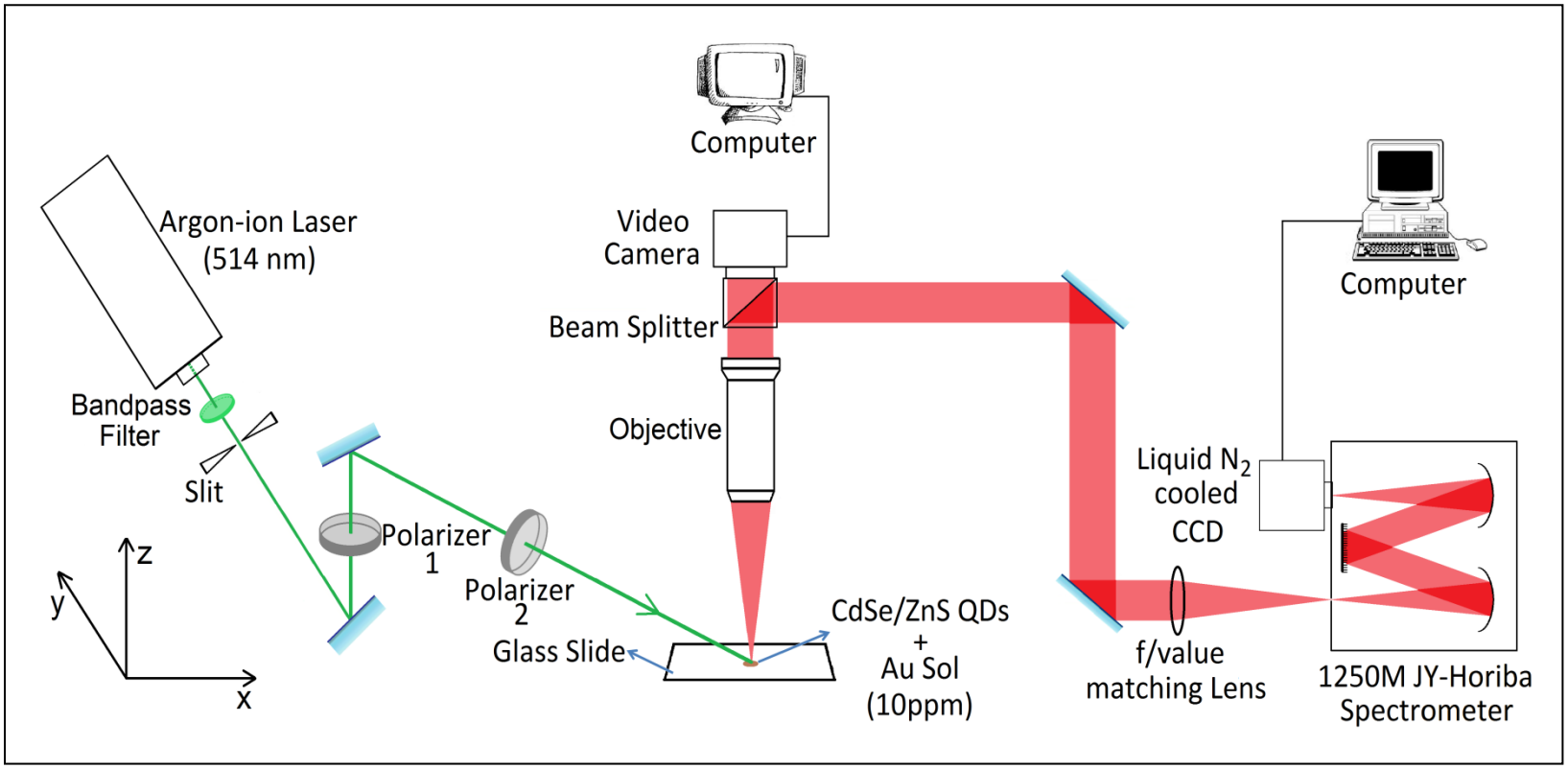

Figure 3.2 Experimental setup for PL intensity determination with variation in Incident intensity using Polarizers

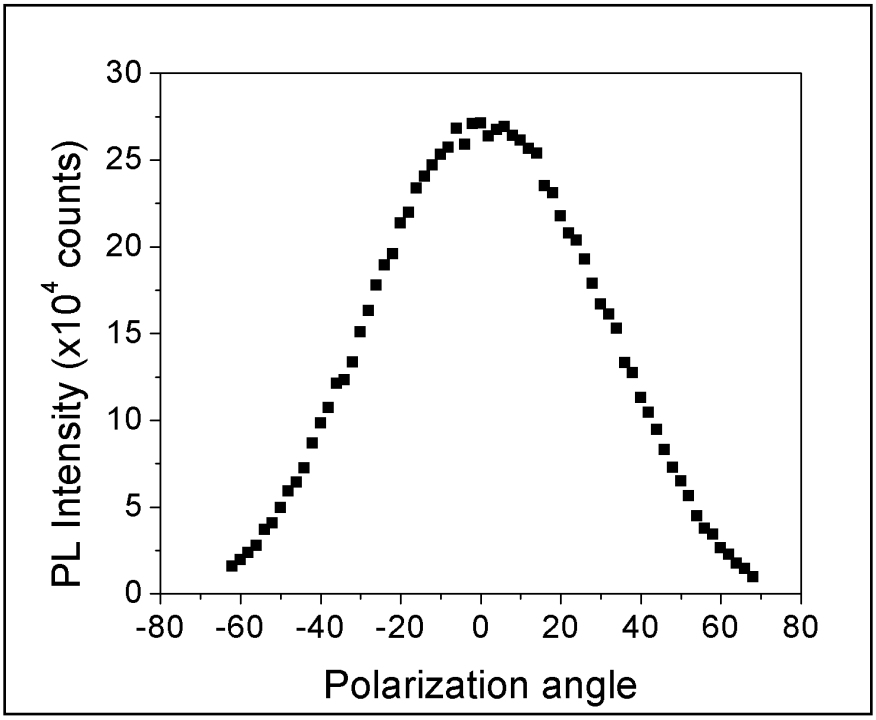

Figure 3.3 Variation in PL intensity from sample with Polarization angle of polarizer # 1

Using these two arrangements, # 1 and # 2, only scattered intensity and PL intensity data were obtained. But, the main objective was to determine the nature of PL with change in incident intensity of the laser. For this, the incident intensity of the laser beam also had to be determined. The arrangement # 2 was, therefore, modified by placing a plane glass slide in the path of laser between polarizer 2 and the sample. This glass slide was kept at certain angle other than normal to the laser beam so that part of the laser gets transmitted through this glass slide and part of it gets reflected from the surface of glass slide. The reflected part of the beam is made to enter the spectrometer to determine its intensity. Using this arrangement, the scattered intensity can be calibrated with the intensity of the reflected part of the beam. In order to get the actual relation between the incident and scattered beam, the intensity of the beam getting transmitted from the glass slide has to be measured. To measure this intensity, a mirror was placed in path of beam between the glass slide and the sample. This mirror reflects the

transmitted part of beam such that it enters into the spectrometer following the optics. Thus, the intensity of both these beams is determined. Using these two values, the reflectivity of glass slide was determined and actual relation between the incident intensity and the scattered beam was determined.

3.3 Experimental Setup for Surface Plasmon measurements

The setup for determination of effect of surface plasmons on PL from QDs, called as arrangement # 3, can be divided into two parts. The first part was used to get both s- and p-polarized beams while the second part was used to create plasmons using Kretschmann configuration without goniometer. In the first part, the laser is passed through a band pass filter, to allow only 514 nm wavelength to pass through, while blocking all other radiations. This beam is then passed through a thin slit to get a thin collimated beam which is then bifurcated into two beams, namely, B1 and B2, using Beam Splitter (BS1).

The laser coming from the source is already polarized along an angle near to the vertical direction (z-axis) which using a polarizer was converted into p-polarized beam before hitting the prism. This p-polarized beam has polarization perfectly along z axis. Since, the polarization angle difference between the original beam and p-polarized beam was small (≤5°); there was not much decrease in the intensity of the p-polarized beam as compared to the original beam. But, when the same beam was made s-polarized, the intensity of the s-polarized beam dropped by a huge factor because the polarization angle difference between the original beam and the s-polarized beam was large (≥85°). In order to get almost same intensity for s- and p-polarized beams, a combination of two Beam Splitters (BS) and five mirrors (M) was introduced. BS2 bifurcates B1 in two parts. The beam which goes straight through BS2, after reflection from M1 and M2, goes into BS3 and gets reflected along x-direction. The polarization angle of this beam remains the same as that of original beam. However, the part of B1 which was reflected from BS2 undergoes reflection from three mirrors (M3, M4 & M5) before hitting BS3. While getting reflected from these three mirrors (M3, M4 & M5), the direction of

polarization of the beam gets changed by 90°. Thus, this beam has polarization perpendicular to that of the first part. After passing through BS3, these beams propagate along x-direction overlapping each other and further collimated together using a 500 micron slit. This collimated beam is then passed through P3 which ultimately decides the polarization angle of the final beam before hitting the prism.

The second part of the setup starts from mirror M6. The collimated polarized beam after reflection from M6 hits the prism as shown in figure 3.4 and after getting reflected from base of the prism goes to M7 and then M8. The prism is coated with 35 nm Au film at its base and a thin layer of QDs is deposited on this Au film. This Prism is kept stationary such that the base of the prism is along the horizontal plane (x-y plane). The mirror M6 has a circular calibrated scale to measure its orientation (degrees) and is placed on a stage which can move along x-direction. Mirrors M6, M7 and M8 have their rotation axis along y direction.

The beam hitting M6 is in x-direction (horizontal) and after reflection from M6 hits the prism at a desired angle and after reflection from its base (assuming that the angle of incidence at the base of the prism is after critical angle), comes out of the prism at the same angle and hits mirror M7. M7 is rotated such that the beam after reflection hits the center of M8, which is then rotated such that the reflected beam after passing through BS4 goes into the spectrometer following the optics as shown in the figure 3.4.

By knowing the angle of M6, the angle of the beam at the prism base can be determined using the calibration discussed later. The spot of the beam at the prism base can be moved to prism center by translating M6 along x-direction. Once the reading is taken at a particular angle, M6 can be rotated to another desired angle and for the beam to hit the same spot as before, at the prism base, M6 can be translated again along x-direction. The beam which comes out from the other face of the prism after reflection hits M7 at an angle other than the previous angle. So, M7 can be rotated such that the reflected beam hits the center of M8 again and this M8 can further be rotated to make the beam pass through BS4 and ultimately

into the spectrometer. Thus, a number of readings can be taken by changing the orientation of M6.

At each and every angle, M6 has to be translated along x-direction to bring the beam spot at the same position as before at the base of the prism. In order to make sure that the beam hits the same spot every time, a microscope (Leica S6) has been added which is kept along y-z plane, perpendicular to the plane of paper as shown in figure 3.4. This microscope focuses the area near the first beam spot and has an internally calibrated scale which helps to ensure that the beam spot remains at the same position.

The objective placed above the base of the prism focuses the beam spot and all the radiations which it receives from prism base, either PL (~622 nm) or scattered beam (~514 nm), and sends it to BS4, from where, part of it goes into the video camera and rest of it goes into the spectrometer.

The second part (B2) of the original beam, reflected from BS1, after going through the optics as shown in figure 3.4, hits the beam spot at prism base from back side. Its intensity can be varied by changing the orientation of polarizer P1 while keeping P2 at a fixed orientation. The fixed orientation of P2 ensures that the orientation of the beam hitting the sample from back side remains same throughout the experiment.

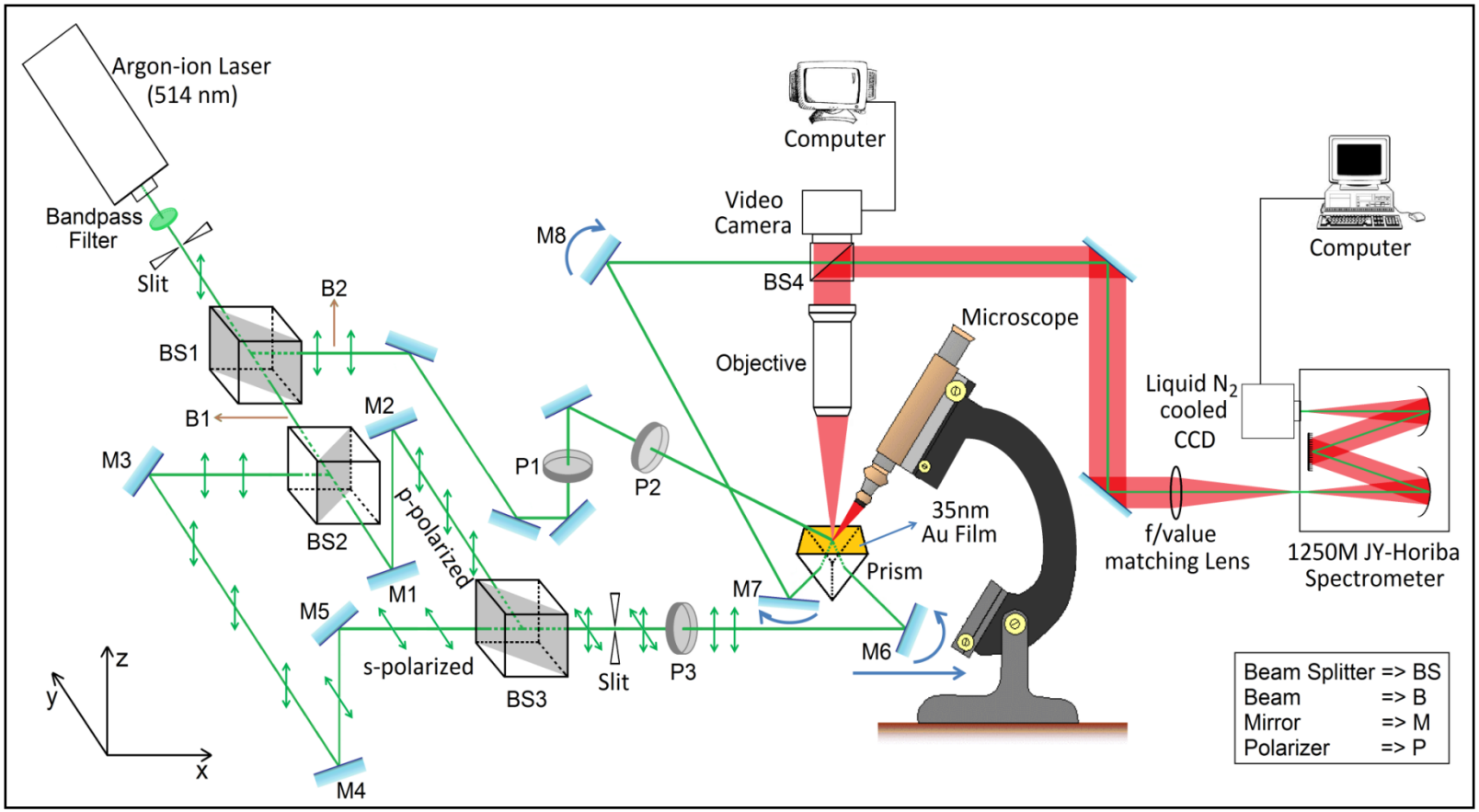

Figure 3.4 Experimental setup for determination of PL from sample in presence of Surface Plasmons

3.4 Determination of angle of the beam at prism base (φ)

The mirror M6 is calibrated in arrangement # 3. Figure 3.4 represents the arrangement of the mirror (M6) and prism. While fixing the prism and laser, care was taken to make sure that the laser incident at A and the Prism base remains parallel i.e. along horizontal as shown in figure 3.5. The laser incident on M6 at A, after reflection, enters the prism at B and gets reflected from the base of the prism at C. The corresponding angles are represented in the figure 3.5. The refractive index of the prism (n_p) is 1.7847. Using Snell's law, the angle of the beam at prism base (φ) has been determined and the calculation is shown in Table 3.2.

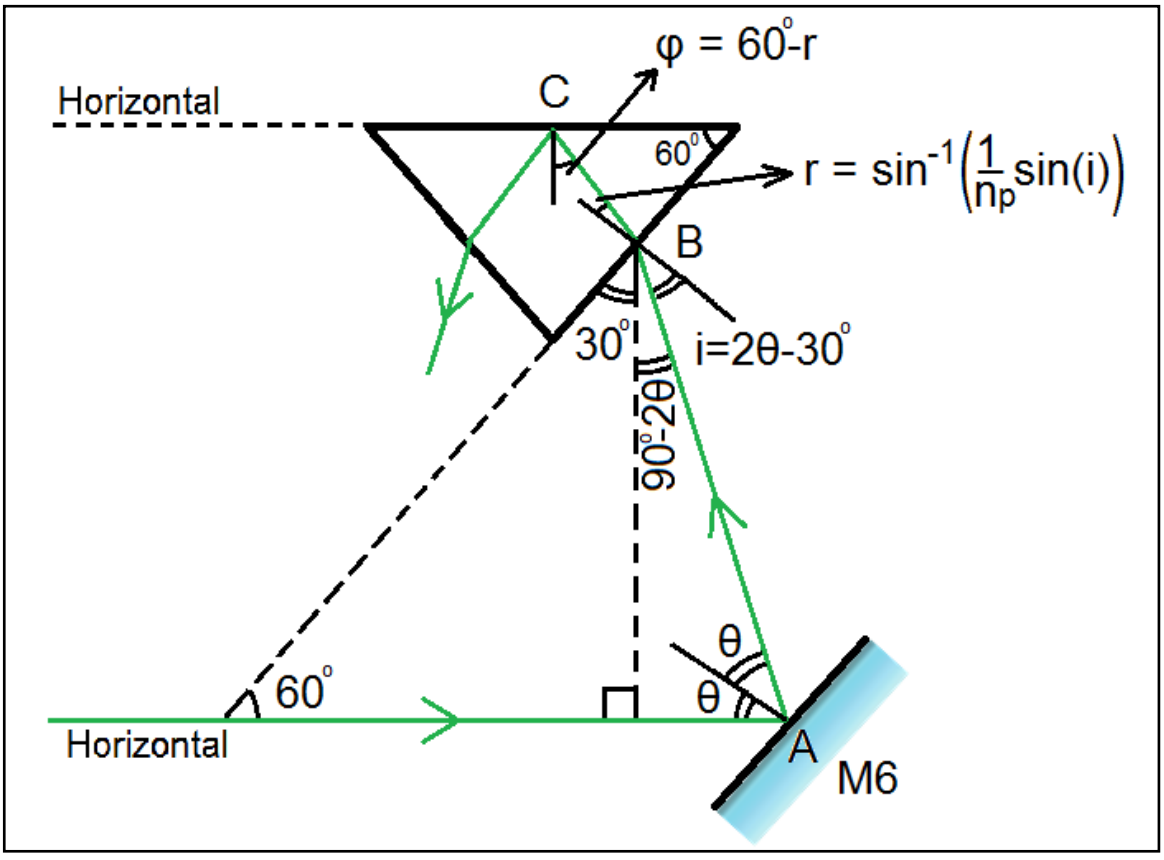

Figure 3.5 Angle determination of laser beam angle at Prism base

Table 3.2 Angle determination of laser beam at Prism base

θ	2θ	i=2θ-30	$r = sin^{-1}\left\{\frac{1}{n_p}\sin(i)\right\}$	Angle @ Prism Base (φ = 60-r)
43	86	56	27.68346662	32.31653
42	84	54	26.95960761	33.04039
41	82	52	26.20512605	33.79487
40	80	50	25.42140014	34.5786
39	78	48	24.60980313	35.3902
38	76	46	23.77169841	36.2283
37	74	44	22.90843535	37.09156
36	72	42	22.02134587	37.97865
35	70	40	21.11174163	38.88826
34	68	38	20.18091189	39.81909
33	66	36	19.23012191	40.76988
32	64	34	18.26061185	41.73939
31	62	32	17.27359619	42.7264
30	60	30	16.27026349	43.72974
29	58	28	15.25177662	44.74822
28	56	26	14.21927316	45.78073
27	54	24	13.17386626	46.82613
26	52	22	12.11664555	47.88335
25	50	20	11.04867843	48.95132

3.5 Advantages of Surface Plasmons measurement Setup

SPR determination using Kretschmann configuration has been used by several groups and this configuration has been modified as per requirement [37]. Our group has also used this configuration to determine the existence of surface plasmons in a liquid crystal containing Au NPs [38]. While carrying out this experiment, it was observed that the beam spot hitting the base of the prism does not remain stationary with changing angles; instead, it translates towards one of the edges of the prism at higher base angles. In such cases, in order to get a good quality data, the Au film at the base of the prism has to be uniform throughout.

The setup shown in figure 3.4 as arrangement # 3 overcomes this issue. The prism in this arrangement is kept stationary with a microscope objective at the back side focusing at a point at its base. Mirror M6 is used to change the angle of the beam at the prism base. The beam spot can be moved to the same spot after changing the angle of M6 by moving this mirror along x-direction. Since, only plane mirrors are used throughout the arrangement, the laser beam always remains parallel. Prism can be translated along the horizontal plane (x-y plane) to move this focal point to different spots or even to scan the surface of film/sample at prism base. The video camera attached takes the live image of the sample. The spectrometer analyses the intensity and spectral distribution of the incoming signal. The beam B2 which hits the sample at inclined angle acts as the control beam to excite the sample with desired intensity. The optical microscope adds to the ability to hit the sample or the prism base at the same spot.

3.6 Raman Spectroscopy measurements

Raman spectroscopy was carried out using Horiba Jobin Yvon LabRAM Aramis Raman Spectrometer which is equipped with Czerny-Turner spectrometer, confocal microscope and multiple laser sources including HeNe, Ar-ion, solid state and diode lasers [39]. Sample # 1, Sample # 2 and Glass slide were analyzed by using this spectrometer with 473 nm (blue) diode laser as the excitation source.

3.7 UV-VIS Absorption measurements

The absorbance spectrum of 10 ppm Au solution was measured using UV-3600 UV-Vis-NIR Spectrophotometer which uses tungsten lamp as radiation source and PMT detector (Photomultiplier tube) in visible region [40]. The absorbance spectrum was measured from 400 nm to 800 nm. The emission spectrum for the same sample was measured using solid state laser, with emission peak at 532 nm as the excitation source, and JY Horiba Triax-550 spectrometer, with CCD detector for emission peak determination [38].

CHAPTER 4

RESULTS AND DISCUSSION

This chapter can be divided into two sections. In the first section, the behavior of PL, in terms of intensity and peak position, with respect to the changes in incident laser intensity is discussed. In the second section, the evidence of surface plasmon resonance using 35 nm Au film at prism base is presented followed by a series of simulations supporting the data. The nature of surface plasmon resonance in presence of thick and thin film of CdSe/ZnS QDs over this 35 nm Au film is presented. Using bilayer film, Au layer and QDs layer, the effect of surface plasmon electric field on the PL behavior of QDs is presented and discussed.

4.1 PL measurements

Figure 4.1 and 4.2 represent the absorption and emission spectrum of 10 ppm Au NPs, respectively. The absorption peak is at ~526 nm and emission peak is at ~634.5 nm which is a confirmation that the particle size of Au NPs is 14 nm [27].

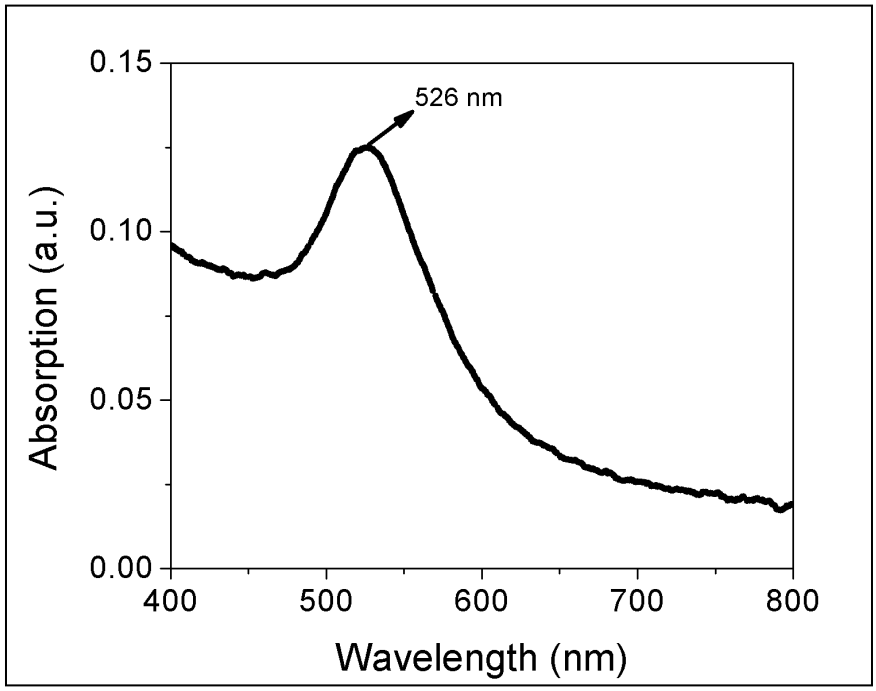

Figure 4.1 Absorption spectrum of 10 ppm Au NPs

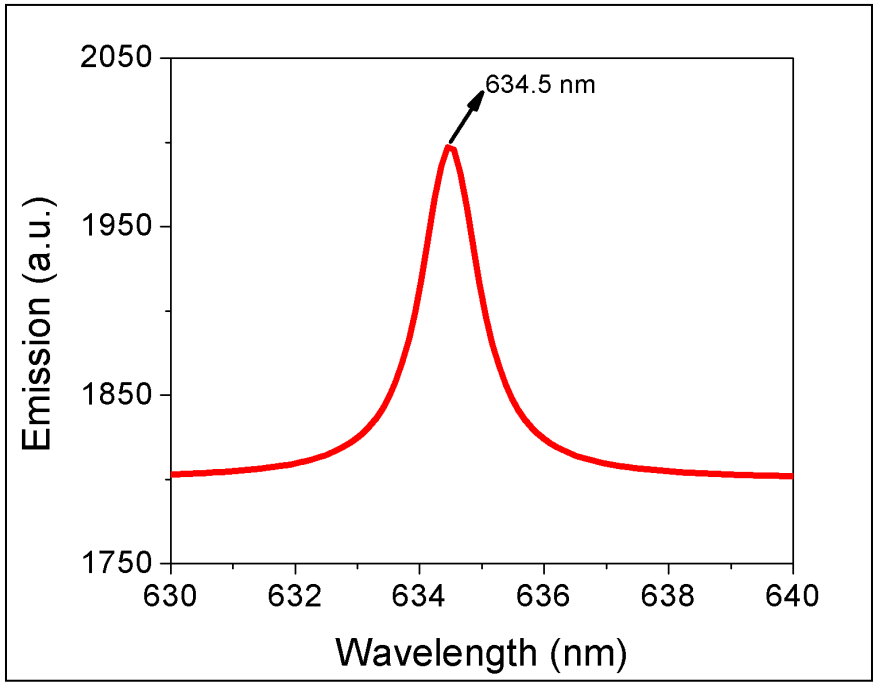

Figure 4.2 Emission spectrum of 10 ppm Au NPs

Figure 4.3 shows nature and peak position of the Incident laser which is used as an excitation source throughout the experiments having peak position at 514.05 nm with full width half maximum (FWHM) of 0.106 nm. Figure 4.4 represents the PL curve for CdSe/ZnS QDs having peak position at 621.86 nm with FWHM of 18.16 nm.

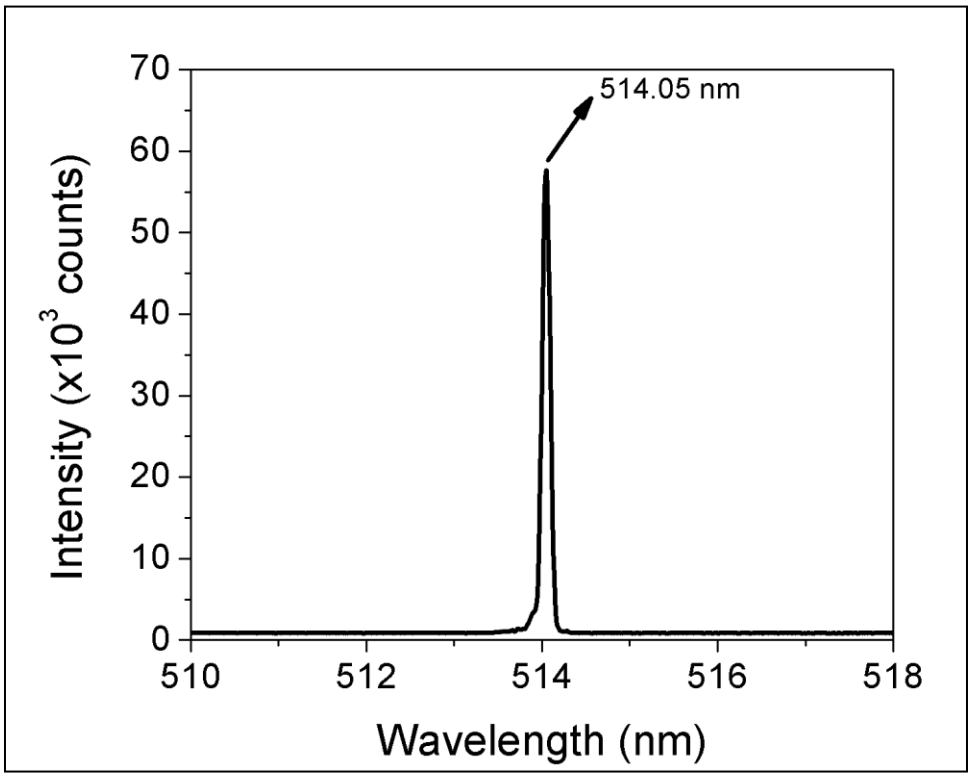

Figure 4.3 Nature of Incident Laser

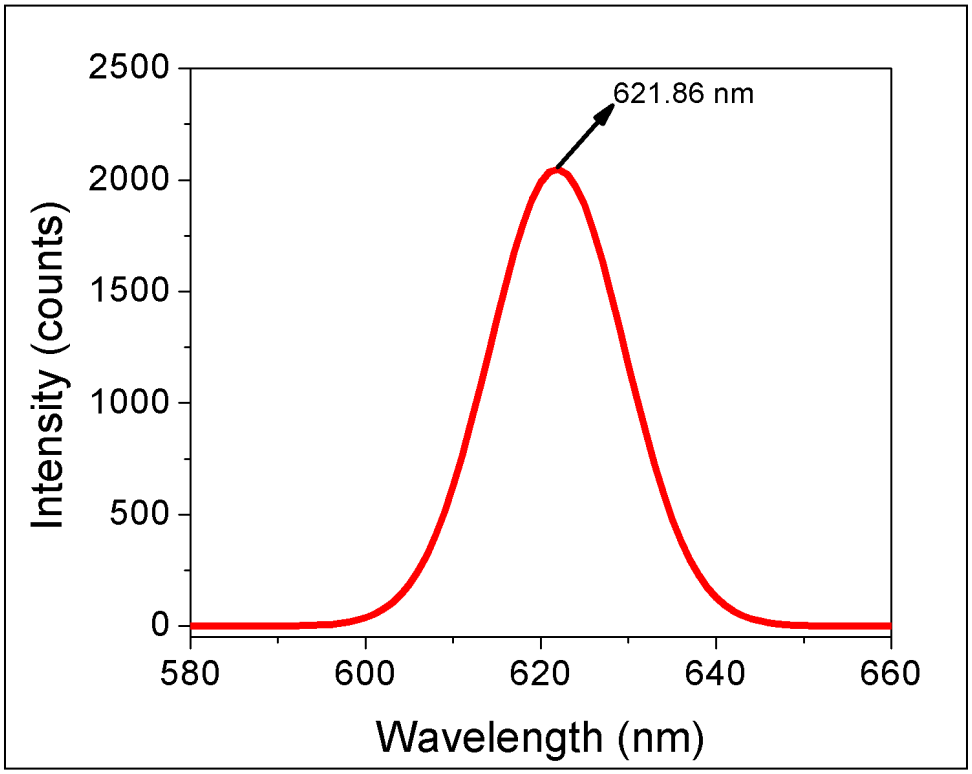

Figure 4.4 Nature of PL from CdSe/ZnS QDs

As discussed earlier, two samples were prepared for PL measurements. These measurements were initially carried out using configuration # 1. The PL intensity variation and shift in PL peak position with change in incident intensity using OD filters is shown in figure 4.5 and 4.6.

It can be observed from the previous two figures that the number of data points obtained using filters is quite less. More number of data points increases the reliability of results. In order to increase the number of data points, the OD filters were replaced by two polarizers as discussed in earlier for configuration # 2. Using this configuration, the variation in PL intensity and PL peak position were obtained as shown in figure 4.7 and 4.8, respectively.

From these four curves, shown in fig. 4.5, 4.6, 4.7 and 4.8, it can be concluded that the PL intensity varies linearly with Incident intensity and it gets enhanced by 2-3 times with addition

of Au NPs to pure QDs. The PL intensity is depends upon the radiative recombination of the excitons [41]. The addition of Au NPs results in the excitation of LSPs which eventually results in enhancement of the localized electric field. The local-field enhancements associated with LSPs allows metal nanostructures to act as nanoscopic antennas that ultimately enhances light absorption, and also affect the radiative and non-radiative decay of the nearby photoluminescent particles [42, 43]. Resultant quenching or enhancement of PL is determined by the competition between excitation enhancement, emission enhancement and PL quenching [42, 43]. Increase in PL intensity by a factor of ~3, as shown in figure 4.5 and 4.7, can be due to the presence of Surface Enhanced Raman Spectroscopy (SERS) active Au NPs in the proximity of QDs [44]. As Au NPs are much larger than QDs, the scattering component can be dominant over absorption which may increase the resultant PL [45].

With increase in incident excitation intensity, the recombination of carriers in the excited states can get enhanced due to the band filling of QDs. The blue shift, shown in figure 4.6 and 4.8, might be the result of this band-filling effect [46, 47]. Also, with the addition of Au NPs, there is further increase in blue shift which can be due to increase in localized electric field due to excitation of LSPs.

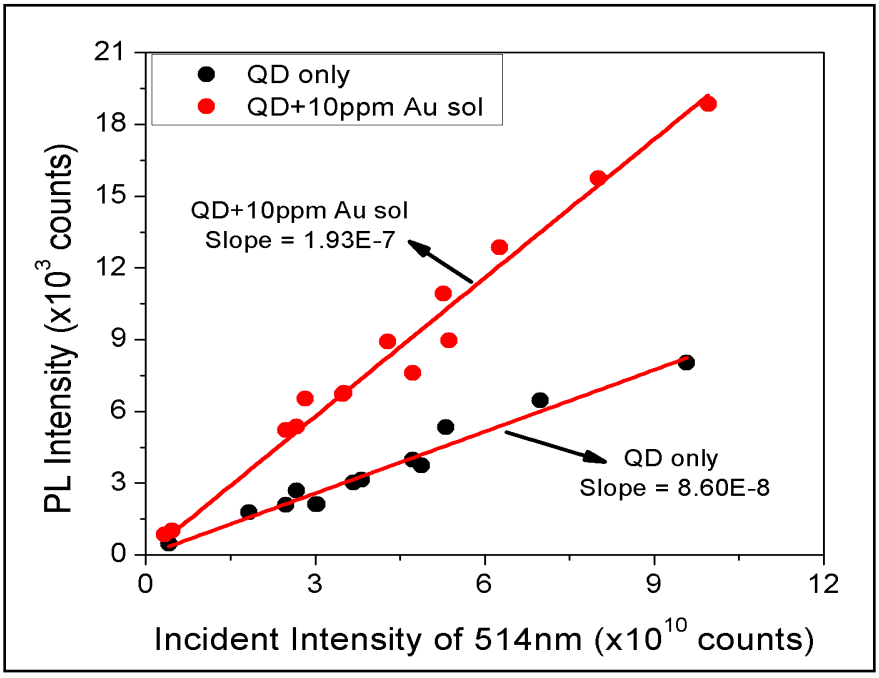

Figure 4.5 PL Intensity variation w.r.t. Incident Intensity using OD filters

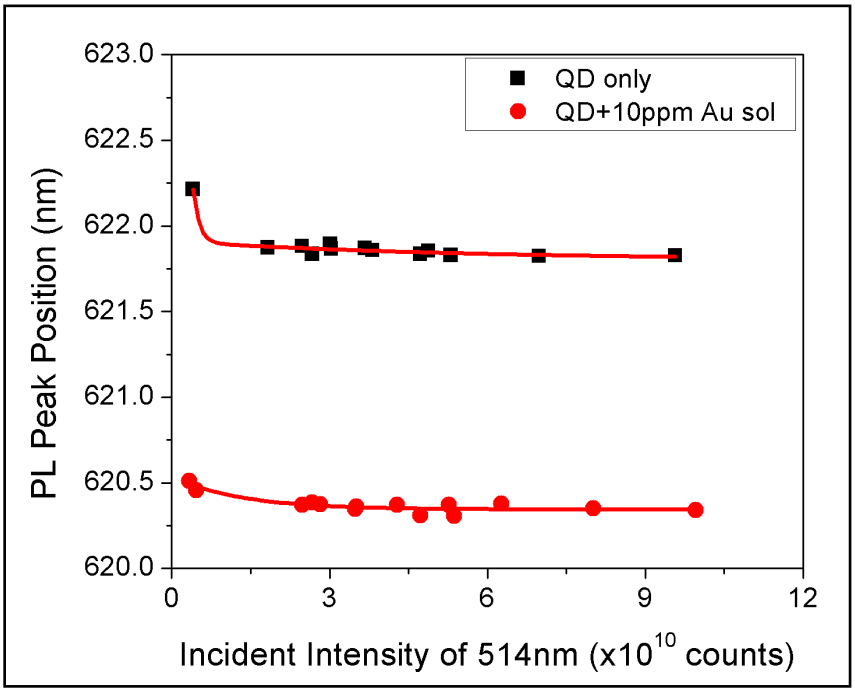

Figure 4.6 Shift in PL peak position w.r.t. Incident Intensity using OD filters

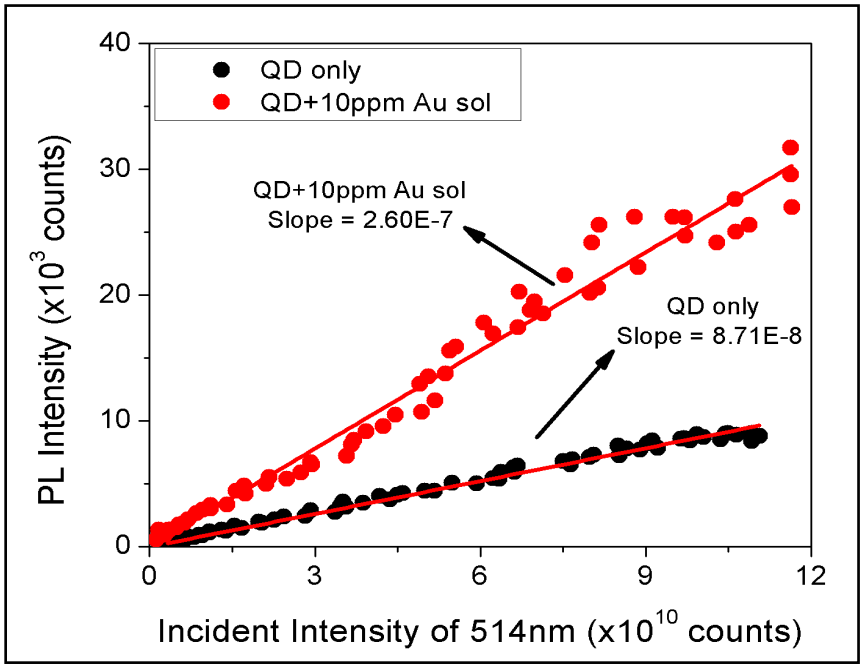

Figure 4.7 PL Intensity variation w.r.t. Incident Intensity using polarizers

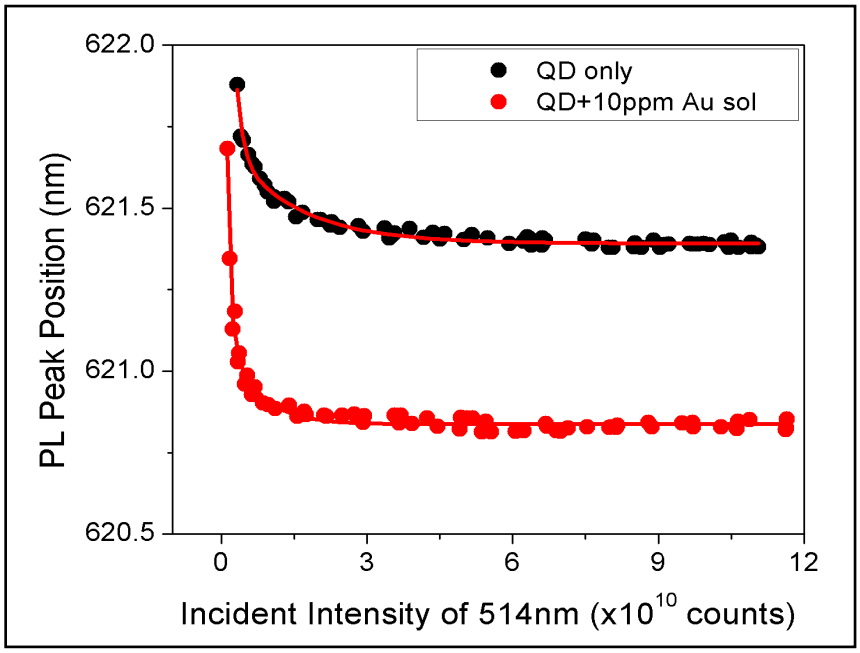

Figure 4.8 Shift in PL peak position w.r.t. Incident Intensity using polarizers

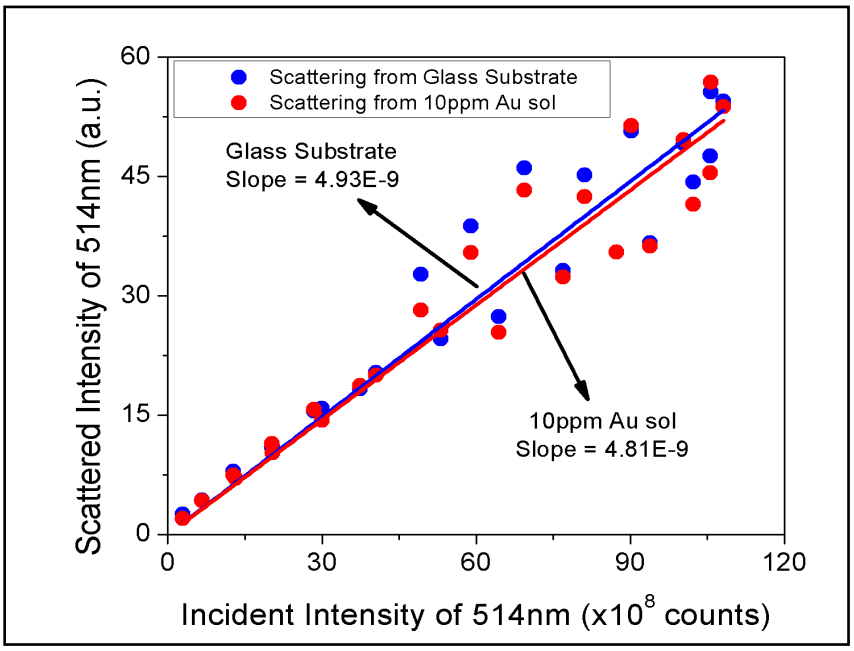

Figure 4.9 Scattering contribution from Glass substrate and Au NPs

Figure 4.9 shows the scattering from Glass substrate and 10 ppm Au sol dried over plane glass substrate. The values of slopes for scattering from these two are very small. This means that their contribution in the scattering of sample #1 and # 2 can be neglected. Also, Au NPs do not show significant scattering macroscopically as the slope in figure 4.9 are almost equal.

4.2 Effect of SPPs on PL from CdSe/ZnS QDs

4.2.1 Creation of surface plasmons

In order to observe the PL behavior of QDs in the presence of surface plasmon polaritons, arrangement # 3 was employed as shown in figure 3.4. Surface plasmons are generated using Kretschmann configuration with a 35 nm Au film at base of a high index prism (n_p = 1.7847, critical angle = 34.08°). The reflected intensity measurements were made by varying the incident laser angle at the base of the prism from 32° to 49°. The nature of reflected laser from prism base, for both s- and p-polarized laser beams, is shown in figure 4.10 and

4.11. In case of s-polarized beam, there is not much change in reflected intensity for all angles. However, in case of p-polarized beam, the reflected intensity drops by a factor of 80% at φ = 49°. This decrease in reflected intensity for p-polarized beam represents the creation of plasmons and is called as surface plasmons resonance (SPR) dip. More loss in reflected intensity means higher value of surface plasmon electric field.

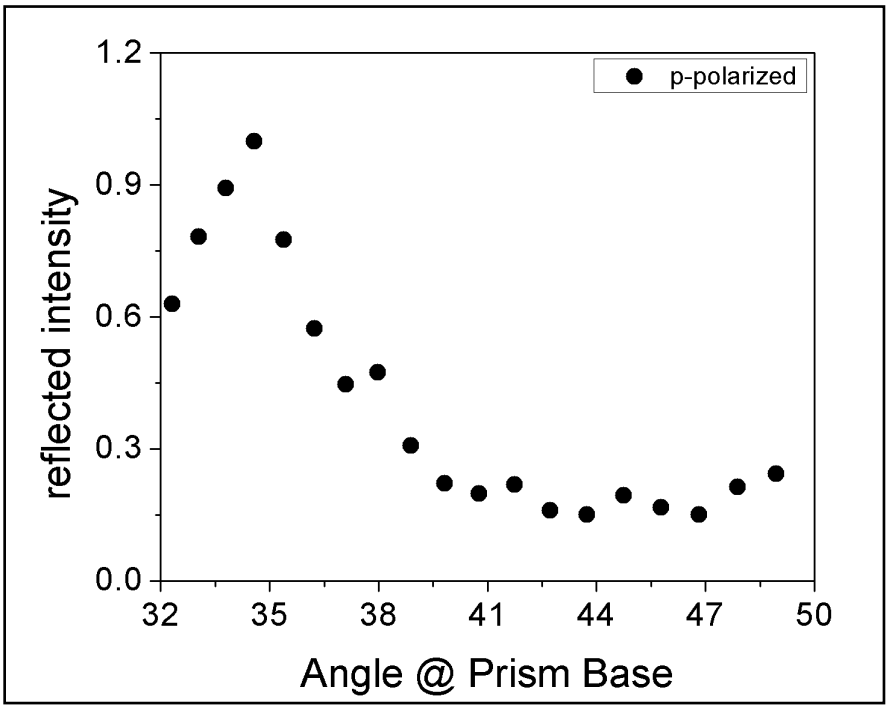

Figure 4.10 Reflectivity of p-polarized beam from Prism base showing evidence of SPR

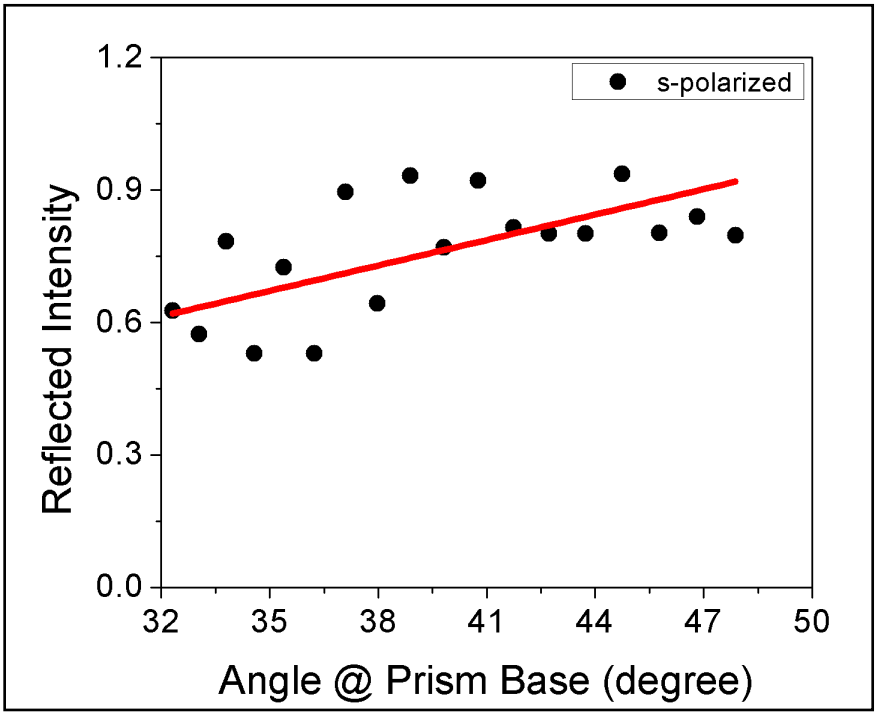

Figure 4.11 Reflectivity of s-polarized beam from Prism base showing no SPR

Usually, the dip obtained for SPR is very sharp [48]. However, in this case, the resonance dip is very wide. This can be due to higher value of the imaginary part of dielectric function of Au. Figure 4.12 shows a series of simulations using the equations from reference [48], as shown below.

$$R = \left| \frac{e^{(-i2\emptyset_{21})} - e^{(-i2\emptyset_{01})} e^{(-2\alpha_1 d)}}{1 + e^{[-i2(\emptyset_{21}+\emptyset_{01})]} e^{(-2\alpha_1 d)}} \right|^2 \quad (30)$$

$$\emptyset_{01} = tan^{-1}\left(\frac{\varepsilon_0 \alpha_1}{\varepsilon_1 k_0}\right)$$

$$\emptyset_{21} = tan^{-1}\left(\frac{\varepsilon_2 \alpha_1}{\varepsilon_1 k_2}\right)$$

$$k_j = \left(k_0^2 \varepsilon_j - \beta^2\right)^{\frac{1}{2}}$$

$$\alpha_1 = (\beta^2 - k_0^2\varepsilon_1)^{\frac{1}{2}}$$

$$\beta = k_0\sqrt{\varepsilon_2}sin\varphi$$

Where, the subscripts 0, 1 and 2 represent the quantities in air, metal and prism, respectively. k_j is the wave vector component in a direction perpendicular to the interface in the medium j, α_1 is the attenuated coefficient of the field in the metal, β is the component of the incident wave vector parallel to the interface and k_0 is the wave number ($2\pi/\lambda$) for the wavelength λ in free space. The complex dielectric constant of metal is given by $\varepsilon_1 = \varepsilon_r + i\varepsilon_i$, where, ε_r is the real part and $i\varepsilon_i$ is the imaginary part. From figure 4.12, it can be observed that with increase in the value of imaginary part of the dielectric function of Au, the width of the SPR dip also increases. From the literature [49], the value of dielectric function of Au for 514 nm wavelength is ~ -3.33+i2.93. But, when equation (30) was fitted with the experimental data, the value of dielectric constant for Au is determined to be -3.33+i6.93. The defects present in the material greatly affect its dielectric function. So, the increase in imaginary part of the dielectric function of Au might be due to the defects created in the film during deposition.

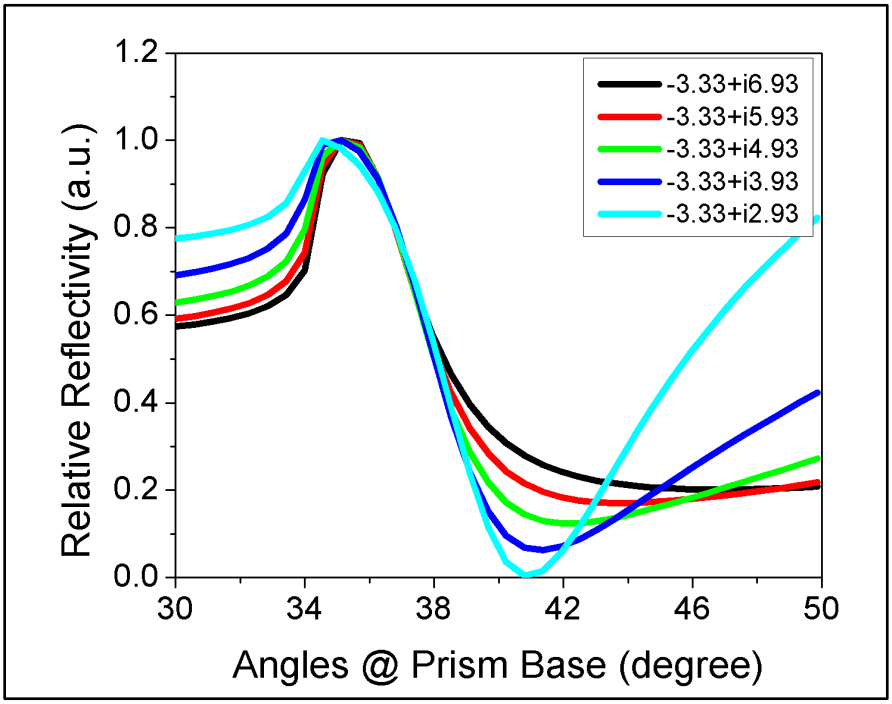

Figure 4.12 Simulation curves showing change in the nature of SPR with variation in imaginary part of dielectric constant of Au

4.2.2 Effect of SPPs on PL from thick film of CdSe/ZnS Quantum Dots

Initially, a thick film of QDs was deposited over the 35 nm Au film at prism base by dissolving QDs in chloroform. In the beginning, when there was no sample at the back of Au coated prism, the coupling condition was created after TIR. TIR takes place because the refractive index of air is lower than that of the prism. The refractive index of CdSe/ZnS QDs is ~2.38-2.48 [44]. When thick film of QDs was deposited at the back of the prism, the beam goes from a medium of lower refractive index (prism) to a medium of higher refractive index (CdSe/ZnS film), therefore, TIR takes place at CdSe/ZnS film/Air interface and thus, no significant change in reflected intensity was observed as seen in figure 4.13.

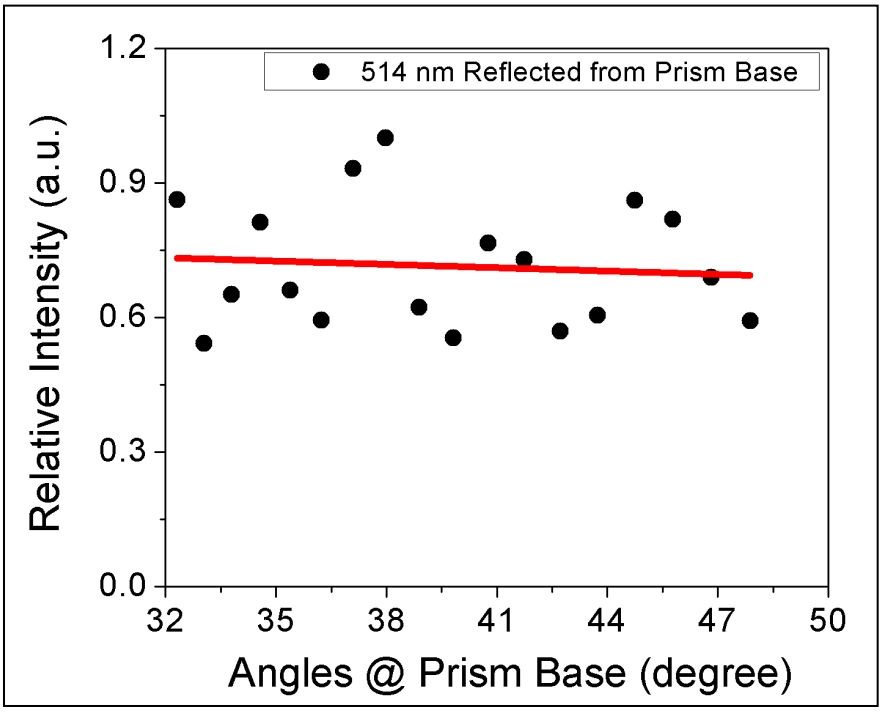

Figure 4.13 Reflectivity of 514 nm laser reflected from Prism base with thick film of CdSe/ZnS QDs deposited on Au film

Using this film, the experiments were conducted further. Figure 1.14 shows the nature of 514 nm wavelength collected from the back side of the prism. It can be observed that the intensity of this 514 nm wavelength decreases slightly at higher angles. This may be due to increase in path length of 514 nm laser beam inside the CdSe/ZnS film at higher base angles.

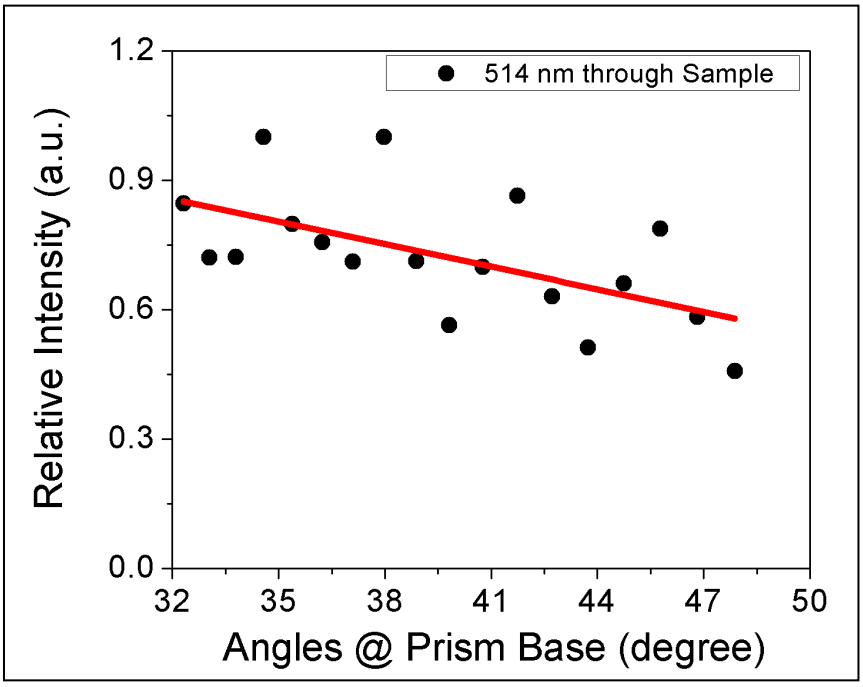

Figure 4.14 Relative Intensity of 514 nm laser passing through the sample and collected from top of Prism base

When the PL was collected from the back side of the prism, the PL intensity is observed to decrease with increasing angle, as shown in figure 4.15. But, if the ratio of this PL and 514 nm intensity is taken, then the curve is found to increase with increasing angles, as shown in figure 4.16. This means that the relative intensity of PL is increasing. This may be due to the fact that more of 514 nm wavelength is getting absorbed at higher angles, as discussed in previous paragraph.

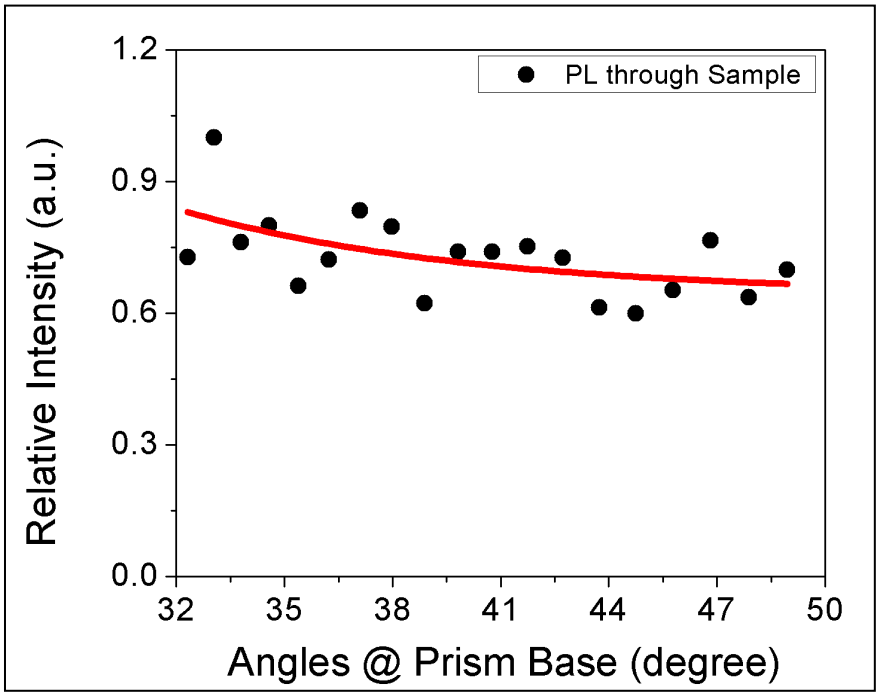

Figure 4.15 PL Intensity from thick CdSe/ZnS QDs film collected from top of Prism base

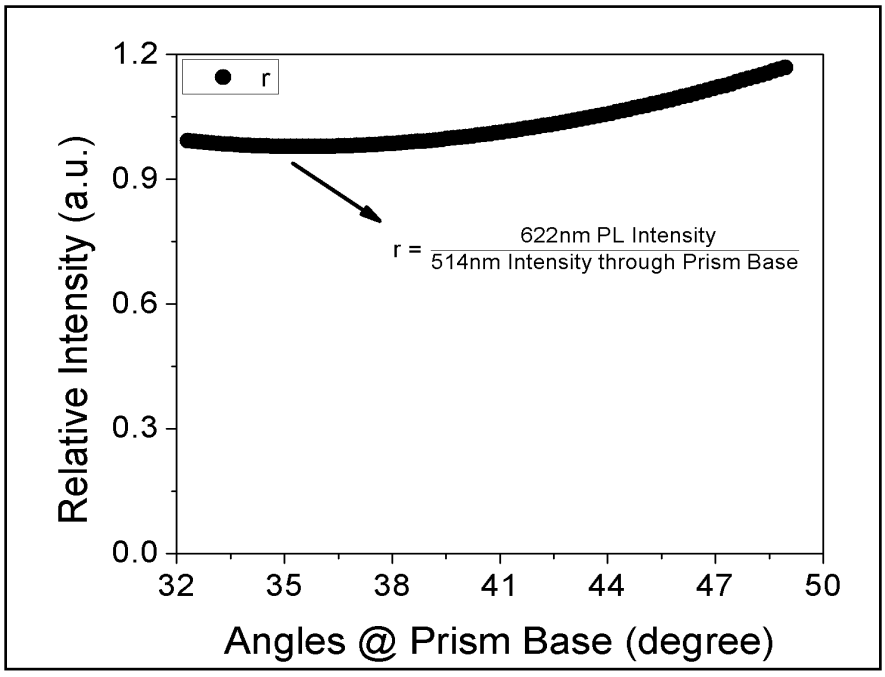

Figure 4.16 Ratio of 514 nm laser and PL Intensity collected from top of Prism base

4.2.3 Effect of SPPs on PL from thin film of CdSe/ZnS Quantum dots

For the formation of thin film of QDs over the 35 nm Au layer, the thick film from the previous section was taken and washed several times using chloroform and water. Then, the SPR measurements were taken using the same setup as before, i.e. arrangement # 3. The reflected intensity of p-polarized laser beam is found to decrease after reflection from the prism base, as shown in figure 4.17, which clearly indicated that surface plasmons are being created.

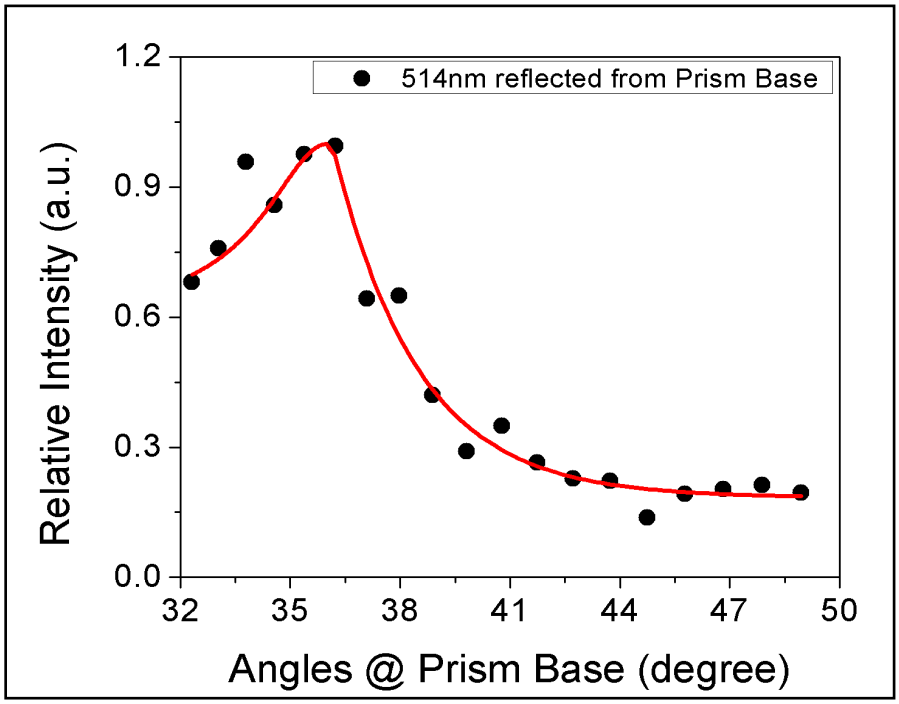

Figure 4.17 Reflected Intensity of 514 nm from Prism base with thin film of CdSe/ZnS QDs deposited on Au film

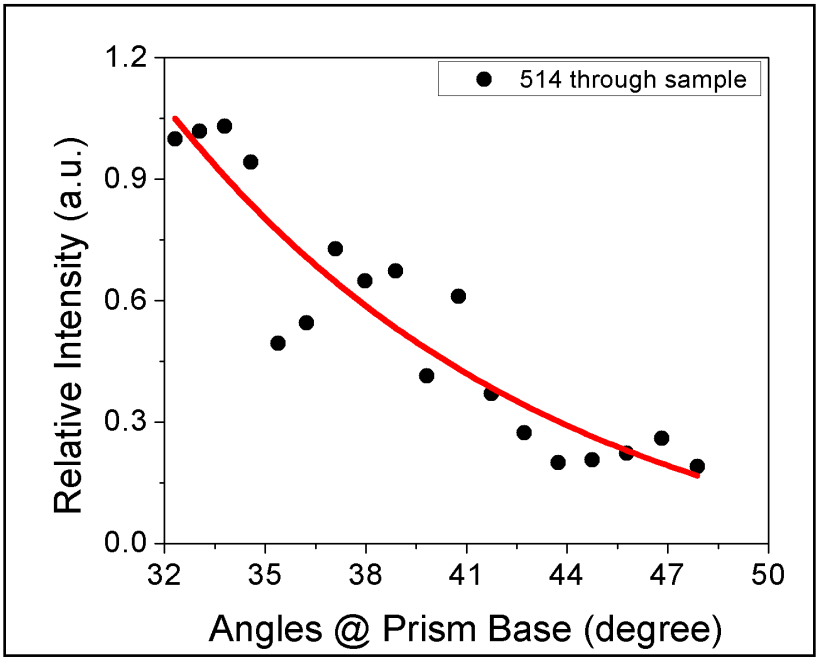

Figure 4.18 Relative Intensity of 514 nm laser, passing through thin film of sample, collected from top of Prism base

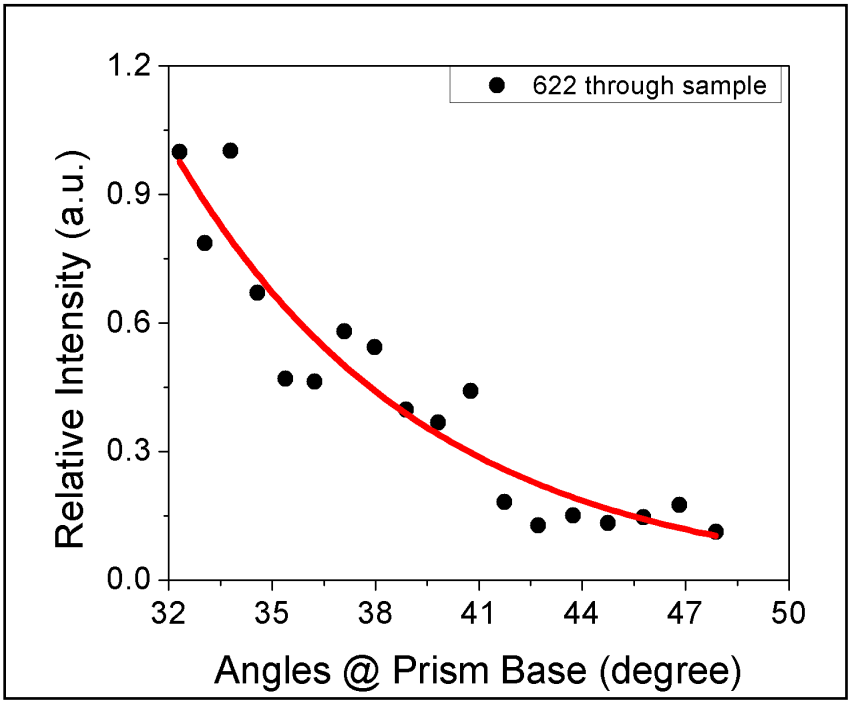

Figure 4.19 PL Intensity from thin CdSe/ZnS QDs film collected from top of Prism base

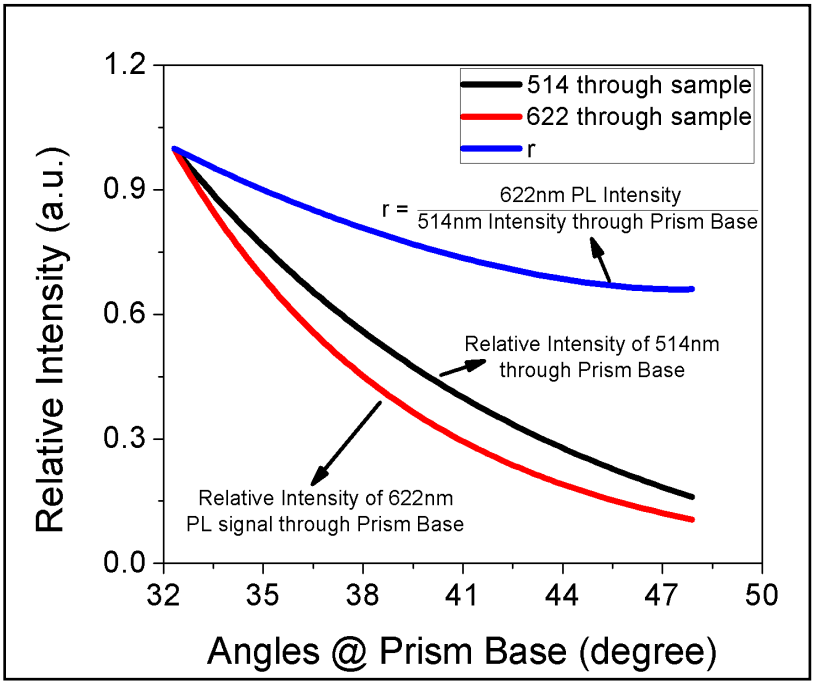

Figure 4.20 Ratio of 514 nm laser and PL Intensity collected from top of Prism base

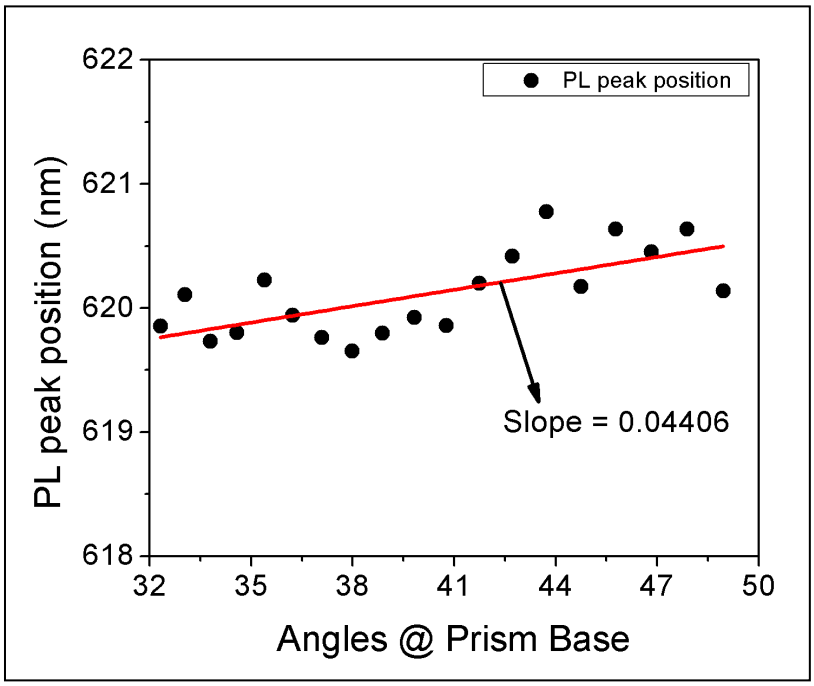

Figure 4.21 Behavior of PL intensity peak position with variation in incident angle of laser beam at Prism base

Now, 514 nm wavelength was collected from back side of the prism. From figure 4.18, it can be observed that the intensity of this 514 nm wavelength decreases with increasing angle. The PL signal is also found to decrease as shown in figure 4.19. When the ratio of the fitted curves for this PL and 514 nm wavelength, collected from back side of prism, was plotted as shown in figure 4.20, it can be seen that the relative intensity of PL goes down, which is in contrast with the previous observation with thick film. This means that the PL signal from this thin film of QDs is getting quenched by the electric field of surface plasmons. The magnitude of SPPs increases with increase in base angle which means that the field associated with them also increases with increasing angle. Due to this continuous increase in electric field, the PL is observed to get reduced with increasing angle. Figure 4.21 shows the nature of PL peak position variation with increasing base angle. From this figure, it can be observed that the PL peak position gets red shifted at higher angles where there is more intensity of electric field associated with SPPs.

Quenching of the PL under the influence of an applied electric field is a common phenomenon. Electrons and holes, having opposite charges, tend to move apart in an external electric field thus, reducing the overlap between their wave functions and lowering the probability of radiative recombination [51]. Destriau et. al. have observed that the perturbations, on the charge carriers, caused by an alternating electric field, are not instantaneous. Out of all the electrons, which are momentarily displaced due to the field, only a certain number return back to their original levels when the field falls to zero. The other electrons, which have been displaced more effectively due to the field, have relatively smaller probability of returning [52]. Thus, the quenching of PL intensity may be due to lowering in the number of available carriers for spontaneous recombination.

The electrons and holes may get localized at positive and negative sides along electric field lines. Thus, the spatial separation might increase the lifetime of the excited photocarriers with growing electric field strength ultimately resulting in the quenching of the QD PL [53].

Under the Influence of external electric field, the potentials in a quantum structure get tilted, causing a shift of the transition energy. This shift is called the quantum confined stark effect (QCSE). In case of type-I systems, there is quadratic red-shift of the transition energy due to QCSE [54]. An electric dipole can be induced in these QDs with the application of an external electric field. As observed in CdSe QDs by Empedocles et. al., red-shift may occur with increase in local fields i.e. larger induced dipole [55]. Thus, at higher angles, as the intensity of SPPs increases, the PL gets red-shifted, as shown in figure 4.21, due to increase in induced dipole as a result of enhanced local electric field.

4.3 Raman analysis for sample # 1 and # 2

Raman analysis for sample # 1 and # 2 was carried out to determine any effect due to SPPs related electric field. Figure 4.22 shows the Raman data obtained from silicon sample which was used just for calibration of the instrument. The peak obtained for silicon sample is at 521.58 cm^{-1}, which matches with the values mentioned in the literature [56].

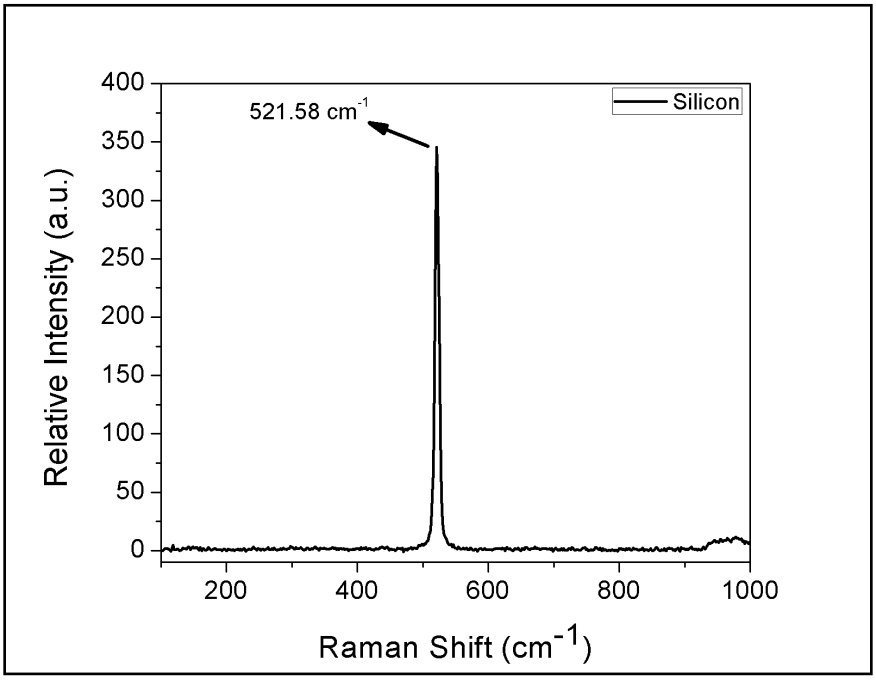

Figure 4.22 Calibration of instrument using Silicon substrate

Figure 4.23 and 4.24 represent the Raman data obtained for Sample # 1, # 2 and clean glass substrate over which the samples were placed. In figure 4.24, the curve obtained for glass has been multiplied by a factor of 20 just to make sure that every peak has been considered. Table 4.3 shows a list of all the Raman bands from the samples (sample # 1, # 2 and glass slide). The bands at 208 and 402 cm^{-1} correspond to CdSe [57] and the band at 277 cm^{-1} corresponds to ZnS [7]. The bands at 707 and 891 cm^{-1} correspond to TOPO [58] and, 504 cm^{-1} band is from glass. The source of bands at 638 and 735 cm^{-1} could not be determined. However, it can be observed from figure 4.23 and 4.24 that the Raman signal gets enhanced by the addition of Au NPs to the QDs matrix. The increase in Raman signal indicates that, due to presence of Au NPs, local electric field is being produced. This supports previously made argument that the blue shift in PL peak position observed for sample # 2, as compared to sample # 1, is due to creation of Localized Surface Plasmons by addition of Au NPs.

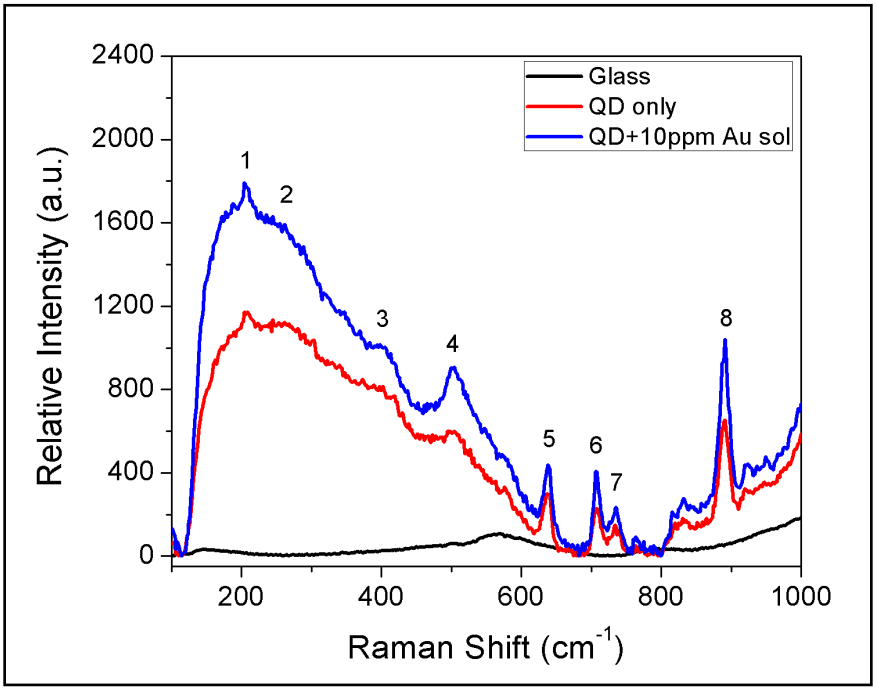

Figure 4.23 Raman Analysis of samples

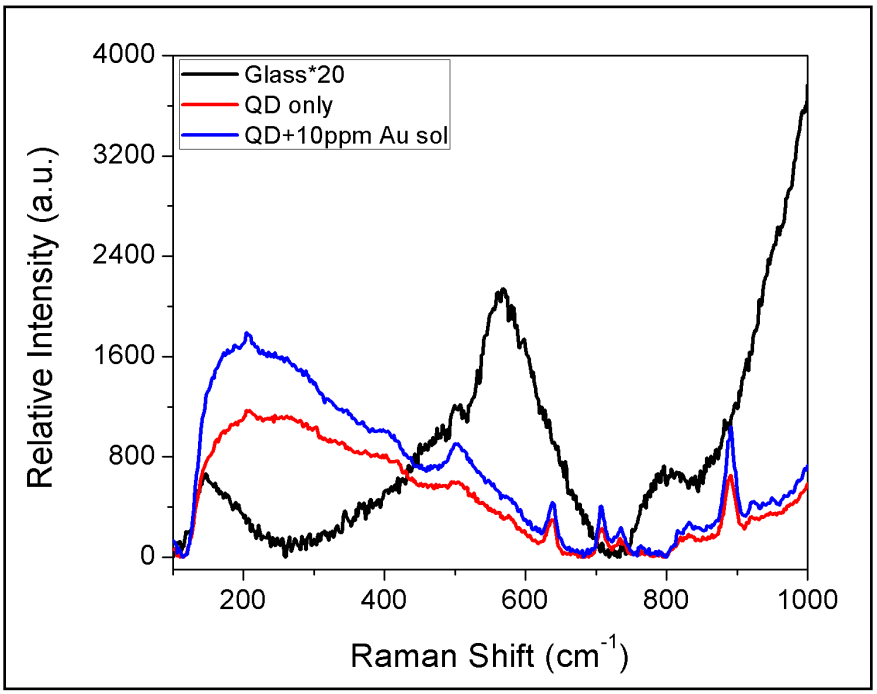

Figure 4.24 Raman analysis of samples, multiplying signal from glass by a factor of 20

Table 4.3 Position of Raman Bands

S.No.	Position of Band (cm^{-1})	Origin of the Band
1	208	CdSe
2	277	ZnS
3	402	CdSe
4	504	Glass slide
5	638	
6	707	TOPO
7	735	
8	891	TOPO

CHAPTER 5

CONCLUSION

PL behavior of CdSe/ZnS core/shell quantum dots has been observed with and without Au NPs. The PL from these QDs varies linearly with incident intensity and is found to get enhanced in the presence of Au NPs. Blue shift in the PL peak position has been observed due to addition of Au NPs to QDs. The addition of Au NPs results in creation of LSPs which greatly enhances the localized electric field thus, causing the blue shift in PL peak position. The PL from QDs should have decreased in the presence of Au NPs but it is found to increase with increase in incident intensity. This means that some other phenomenon, like scattering, is dominating over quenching mechanism of PL.

A novel arrangement for taking SPR measurements using Kretschmann configuration has been designed which has several advantages over conventional system. For example since mirrors are used to change the angle of laser beam at prism base, use of goniometer can be avoided to follow $\theta/2\theta$ relation, rotate prism and detector simultaneously. Also, the prism is kept static which facilitates the use of microscope or any other device to observe the sample in presence of SPR from the back side of prism.

PL from QDs has also been observed in presence of Surface Plasmons created by using a 35 nm Au film coated at the base of a high-index prism. PL signal is found to decrease with increase in magnitude of surface plasmons due to increase in electric field associated with plasmons i.e. the PL from sample gets quenched in the presence of surface plasmons.

REFERENCES

[1] E. Kretschmann, *Zeitschrift für Physik* **241**, 313 (1971)

[2] S. Nie and S. R. Emory, *Science* **275**, 1102 (1997)

[3] C. Langhammer, Z. Yuan, I. Zorić, and B. Kasemo, *Nano Letters* **6**, 833 (2006)

[4] A. Campion and P. Kambhampati, *Chemical Society Reviews* **27**, 241 (1998)

[5] E. C. Le Ru, M. Meyer, and P. G. Etchegoin, *The Journal of Physical Chemistry* B **110**, 1944 (2006)

[6] J. R. Lombardi and R. L. Birke, *The Journal of Physical Chemistry C* **112**, 5605 (2008)

[7] Y. Lee, S. H. Lee, S. Lee, H. Lee, J. Kim and J. Joo, *Applied Physics Letters* **102**, 033109 (2013)

[8] F. D. Stefani, K. Vasilev, N. Bocchio, N. Stoyanova, and M. Kreiter, *Physical Review Letters* **94**, 023005 (2005)

[9] X. Zhang, H. Liu, J. Tian, Y. Song, and L. Wang, *Nano Letters* **8**, 2653 (2008)

[10] X. Huang, S. Neretina, and M. A. El-Sayed, *Advanced Materials* **21**, 4880 (2009)

[11] M. S. Gudiksen, L. J. Lauhon, J. Wang, D. C. Smith, and C. M. Lieber, *Nature* **415**, 617 (2002)

[12] D. J. Norris, A. L. Efros, M. Rosen, and M. G. Bawendi, *Physical Review B* **53**, 16347 (1996)

[13] V. L. Colvin, M. C. Schlamp, and A. P. Alivisatos, *Nature* **370**, 354 (1994)

[14] S. Coe, W. -K. Woo, M. Bawendi, and V. Bulović, *Nature* **420**, 800 (2002)

[15] V. L. Colvin, M. C. Schlamp, and A. P. Alivisatos, *Nature* (London) **370**, 354 (1994)

[16] A. J. Nozik, *Physica E* (Amsterdam) **14**, 115 (2002)

[17] V. I. Klimov, A. A. Mikhailovsky, Su Xu, A. Malko, J. A. Hollingsworth, C. A. Leatherdale, H. -J. Eisler, and M. G. Bawendi, *Science* **290**, 314 (2002)

[18] H. Okamoto, *Japanese Journal of Applied Physics* **26**, 315 (1987)

[19] D. S. Chemla and D. A. B. Miller, *Journal of the Optical Society of America B* **2**, 1155 (1985)

[20] L. L. Chang and L. Esaki, *Physics Today* **45**, 36 (1992)

[21] C. B. Murray, C. R. Kagan and M. G. Bawendi, *Annual Review of Materials Science* **30**, 545 (2000)

[22] P. Reiss, M. Protière, and L. Li, *Small* **5**, 154 (2009)

[23] J. Lia, J. Z. Zhang, *Coordination Chemistry Reviews* **253**, 3015 (2009)

[24] http//en.wikipedia.org/wiki/Core%E2%80%93shell_semiconductor_nanocrystal

[25] http//cms.uni-konstanz.de/en/physik/leitenstorfer/research/ultrafast-quantum-photonics/quantum-physics-with-single-electron-systems-on-molecular-time-scales/

[26] http//micro.magnet.fsu.edu/primer/java/jablonski/lightandcolor/

[27] http//en.wikipedia.org/wiki/Photoluminescence

[28] http//large.stanford.edu/courses/2007/ap272/white1/

[29] http//www.ece.rice.edu/~daniel/262/pdf/lecture10.pdf

[30] http//en.wikipedia.org/wiki/FileSketch_of_surface_plasmon.png

[31] D. Pines and D. Bohm, Physical Review 85, 338 (1952)

[32] R. H. Ritchie, *Physical Review* **106**, 874 (1957)

[33] J. R. Sambles, G. W. Bradbery and F. Yang, *Contemporary Physics* **32**, 173 (1991)

[34] A. Otto, *Zeitschrift für Physik* **216**, 398 (1968)

[35] S. Sharma, J. Murphree, T. Chakraborty, *Journal of Luminescence* **128**, 1771 (2008)

[36] S. M. Sze, *Physics of Semiconductor Devices,* Wiley, New York (1981)

[37] H. S. Chen, J. Y. Wang, S. S. Yeh, C. D. Chen and H. Y. Lin, *Applied Physics Letters* **100**, 011102 (2012)

[38] K. Tiwari, A. K. Singh and S. C. Sharma, *Applied Physics Letters* **101**, 253103 (2012)

[39] www.horiba.com

[40] http//www.ssi.shimadzu.com/

[41] M. Ando, T. J. Inagaki, Y. Kanemitsu, T. Kushida, K. Maehashi, Y. Murase, T. Ota and H. Nakashima, *Journal of Luminescence* **94-95**, 403 (2001)

[42] Y. Chen, K. Munechika, I. J. Plante, A. M. Munro, S. E. Skrabalak, Y. Xia and D. S. Ginger, *Applied Physics Letters* **93**, 053106 (2008)

[43] P. J. Schuck, D. P. Fromm, A. Sundaramurthy, G. S. Kino and W. E. Moerner, *Physical Review Letters* **94**, 017402 (2005)

[44] H. W. Liu, I. R. Laskar, C. P. Huang, J. A. Cheng, S. S. Cheng, L. Y. Luo, H. R. Wang and T. M. Chen, *Thin Solid Films* **489**, 296 (2005)

[45] J. R. Lakowicz, Analytical Biochemistry **337**,171 (2005)

[46] G. Xu, G. Sun, Y. J. Ding, H. Zhao, G. Liu, J. Zhang and N. Tansu, *Journal of Applied Physics* **113**, 033104 (2013)

[47] K. Godo, H. Makino, T. Takai, J. H. Chang, T. Yao, T. Sasao and T. Goto, *Physica Status Solidi (B)* **229**, 439 (2002)

[48] J. H. Gu, Z. Q. Cao, Q. S. Shen and G. Chen*, Journal of Physics D Applied Physics* **41**, 155309 (2008)

[49] R. A. Innes and J. R. Sambles, *Journal of Physics F Metal Physics* **17**, 277 (1987)

[50] S. H. Mohamed and H. M. Ali, *Journal of Applied Physics* **109**, 013108 (2011)

[51] R. Korlacki, R. F. Saraf, and S. Ducharme, *Applied Physics Letters* **99**, 153112 (2011)

[52] G. Destraiu, *Journal of Applied Physics* **25**, 67 (1954)

[53] B. Ullrich, J. S. Wang, and G. J. Brown, *AIP Advances* **2**, 042132 (2012)

[54] M. Larsson, P. O. Holtz, A. Elfving, G. V. Hansson and W. X. Ni, *Physical Review B* **71**, 113301 (2005)

[55] S. A. Empedocles and M. G. Bawendi, *Science* **278**, 2114 (1997)

[56] J. D. Prades, J. Arbiol, A. Cirera, J. R. Morante and A. F. Morral, *Applied Physics Letters* **91**, 123107 (2007)

[57] H. Lange, M. Machon, M. Artemyev, U. Woggon and C. Thomsen, *Physics Status Solidi (RRL) – Rapid Research Letters* **1**, 274 (2007)

[58] http//www.sigmaaldrich.com/spectra/rair/RAIR009323.PDF

BIOGRAPHICAL INFORMATION

Ankit Singh did his Bachelors of Technology from one of the best technical institute from India, Indian Institute of Technology-Banaras Hindu University (IIT-BHU), Varanasi in Ceramic Engineering. During that four year time, he was a summer intern at Indian Institute of Science with his work focusing on Atomic Force Microscopy (AFM) and preparation of polymer nano-composite thin films in 2007 and, preparation carbon nanotubes (CNT) using Chemical Vapor Deposition (CVD) and their application in liquid flow sensors. He is the recipient of Indian Academy of Science (IAS) fellowship, India's most prestigious fellowship at undergraduate level.

He has been involved in research along with Dr. Kuo-Chih Chou at University of Science and Technology (USTB) Beijing, China. His research here involved studying oxidation kinetics of materials like Multi-walled CNTs, SiAlON and AlN whiskers, using Thermogravimetric Analysis (TGA) and modeling of their oxidation behavior.

At University of Texas at Arlington, he is pursuing his M.S. in Materials Science & Engineering working with Dr. Suresh Sharma since fall' 2011. His research here is focused on the study of effect of Surface Plasmon associated Electric Field on photoluminescence from CdSe/ZnS core/shell quantum dots.

After completion of M.S., he will pursue PhD in Materials Science & Engineering from Georgia Institute of Technology and aims at following an academic career afterwards.